Liver SMN restoration rescues the *Smn*$^{2B/-}$ mouse model of spinal muscular atrophy

Emma R. Sutton,[a] Ariane Beauvais,[a] Rebecca Yaworski,[a,b] Yves De Repentigny,[a] Aoife Reilly,[a,b] Monique Marylin Alves de Almeida,[a] Marc-Olivier Deguise,[a] Kathy L. Poulin,[a] Robin J. Parks,[a,c] Bernard L. Schneider,[d,e] and Rashmi Kothary[a,b,c,*]

[a]Regenerative Medicine Program, The Ottawa Hospital Research Institute, Ottawa, Canada
[b]Department of Cellular and Molecular Medicine, University of Ottawa, Ottawa, Canada
[c]Department of Medicine, University of Ottawa, Ottawa, Canada
[d]Brain Mind Institute, Ecole Polytechnique Fédérale de Lausanne (EPFL), Lausanne, Switzerland
[e]Bertarelli Platform for Gene Therapy, Polytechnique Fédérale de Lausanne (EPFL), Geneva, Switzerland

eBioMedicine
2024;110: 105444
Published Online xxx
https://doi.org/10.1016/j.ebiom.2024.105444

Summary

Background The liver is a key metabolic organ, acting as a hub to metabolically connect various tissues. Spinal muscular atrophy (SMA) is a neuromuscular disorder whereby patients have an increased susceptibility to developing dyslipidaemia and liver steatosis. It remains unknown whether fatty liver is due to an intrinsic or extrinsic impact of survival motor neuron (SMN) protein depletion.

Methods Using an adeno-associated viral vector with a liver specific promoter (albumin), we restored SMN protein levels in the liver alone in *Smn*$^{2B/-}$ mice, a model of SMA. Experiments assessed central and peripheral impacts using immunoblot, immunohistochemistry, and electron microscopy techniques.

Findings We demonstrate that AAV9-albumin-SMN successfully expresses SMN protein in the liver with no detectable expression in the spinal cord or muscle in *Smn*$^{2B/-}$ mice. Liver intrinsic rescue of SMN protein was sufficient to increase survival of *Smn*$^{2B/-}$ mice. Fatty liver was ameliorated while key markers of liver function were also restored to normal levels. Certain peripheral pathologies were rescued including muscle size and pancreatic cell imbalance. Only a partial CNS recovery was seen using a liver therapeutic strategy alone.

Interpretation The fatty liver phenotype is a direct impact of liver intrinsic SMN protein loss. Correction of SMN protein levels in liver is enough to restore some aspects of disease in SMA. We conclude that the liver is an important contributor to whole-body pathology in *Smn*$^{2B/-}$ mice.

Funding This work was funded by Muscular Dystrophy Association (USA) [grant number 963652 to R.K.]; the Canadian Institutes of Health Research [grant number PJT-186300 to R.K.].

Keywords: Adeno-associated viral vector (AAV9); Liver steatosis; Peripheral organs; Survival motor neuron; Spinal muscular atrophy

Introduction

Spinal muscular atrophy (SMA) is a neuromuscular disease characterised by loss of alpha motor neurons and muscle atrophy. In most cases SMA is caused by homozygous deletions or mutations in the *survival motor neuron 1* (*SMN1*) gene leading to reduced levels of the survival motor neuron (SMN) protein.[1] Humans have a second, almost identical gene called *survival motor neuron 2* (*SMN2*) which acts as a disease modifier in patients with SMA. However, *SMN2* can only produce 10% full length SMN protein due to a C > T transition within exon 7 that leads to alternative splicing and causes the remaining protein produced to be truncated and rapidly degraded, with a two-fold shorter half-life.[2,3]

There are currently three approved therapies for SMA, adopting variable methods to increase SMN protein production and its delivery: Nusinersen (Spinraza—intrathecal—central nervous system (CNS) predominantly), an anti-sense oligonucleotide and Evrysdi (Risdiplam—oral–systemic) a small molecule, both correct the *SMN2* splicing defect, and Onasemnogene abeparvovec (Zolgensma—intravenous–systemic), an AAV9

*Corresponding author. Ottawa Hospital Research Institute, 501 Smyth Road, Ottawa, ON, Canada K1H 8L6.
E-mail address: rkothary@ohri.ca (R. Kothary).

Research in context

Evidence before this study

Following approval of three drugs that restore SMN protein expression for the treatment of SMA, it is now evident that peripheral and metabolic pathologies remain present in the patient population. Increased lifespan of treated patients requires these additional pathologies to be therapeutically addressed. A large cohort study from paediatric SMA type I-III patients revealed liver steatosis and an increased susceptibility to developing dyslipidaemia.

Added value of this study

To be able to address peripheral pathologies therapeutically, we must first know the individual contribution of each tissue to SMA. Use of a liver tailored AAV9 delivering the *SMN1* gene has enabled us to determine whether a specific peripheral pathology, fatty liver, is due to intrinsic or extrinsic SMN protein depletion and its impact on the whole-body.

Implications of all the available evidence

We demonstrate that peripheral pathologies in SMA could be more impactful on disease outcome than previous work would suggest. Intrinsic restoration of SMN protein in the liver alone was enough to rescue whole-body pathologies in a mouse model of SMA. Extensive research is still required to understand at a molecular level how distortion of SMN protein in the liver is impacting the rest of the body. Our work aligns with present evidence that hepatic steatosis might be a primary defect in SMA.

gene therapy that delivers a copy of the *SMN1* cDNA.[4] Although these therapies improve motor ability and survival of patients with SMA, they are not curative.[4] Furthermore, preclinical and clinical studies demonstrate several of these therapies increase SMN protein in peripheral tissues including the liver, yet the benefit of increased peripheral SMN in tissues such as the liver remains unknown.[5–7]

While SMA is predominantly thought of as a motor neuron disease, there is evidence to suggest SMA pathology extends beyond the CNS to peripheral tissues such as heart, lung, pancreas and liver.[8] High expression of SMN protein in all tissues during embryogenesis suggests most tissues require SMN protein for normal development.[9] Furthermore, a motor neuron specific knockdown of SMN, produces a more modest SMA phenotype than when SMN protein is expressed at low levels ubiquitously.[10] The effect of SMN ubiquitous expression lends itself to suggest inter-organ communication could play a role in SMA pathology.[11] Importantly, one organ central to many whole-body processes is the liver, with hepatokine biology emerging as a potential link to altered metabolism in several other tissues.[12]

Liver defects are evident from birth and before motor pathology in severe SMA mice.[13] Molecular and morphological changes in the liver, specifically erythropoiesis and megakaryopoiesis, are seen at postnatal day (P) 1. These developmental liver defects have the potential to affect a wide-array of systemic tissues.[13] Mouse studies investigating targeted deletion or increased production of SMN protein in the liver demonstrate an important role for this organ in pathology. Deletion of *Smn* exon 7 directed to the liver, which causes a complete loss of SMN protein from this organ, leads to impaired liver development, iron overload and a lack of regenerative capacity in (*Alfp-Cre, Smn*$^{F7/F7}$) mutant mice.[14] This restriction of *Smn* exon 7 deletion to the liver ultimately caused severe atrophy and late embryonic lethality.[14] While this model provides a complete knockout and is therefore not reflective of SMA, it does demonstrate the drastic impact of liver SMN protein depletion and provides strong evidence for the involvement of the liver in SMA disease. Furthermore, *Smn*$^{2B/-}$ mice develop microvesicular steatosis within 2 weeks post-birth, with molecular evidence of fibrosis.[15] This hepatic damage causes dysfunction in coagulation, iron homeostasis and insulin-like growth factor 1 (IGF1) metabolism, highlighting multiple processes impacted by ill liver health.[15] The *Smn*$^{2B/-}$ mice present with a less severe phenotype and have a greater life span (~28 days) compared to other more severe models.[16] Peripheral pathologies, specifically microvesicular steatosis, are well characterised in this model enabling important whole-body pathologies to be investigated.[8,15,17]

Additionally, several studies have now reported on the beneficial impact of systemic delivery of the approved therapies that increase SMN protein production.[18,19] In the Taiwanese SMA mouse model, systemic antisense oligonucleotide (PMO25) restoration of SMN protein ameliorated liver specific defects further affirming a key dependence of the liver on SMN protein.[13] Systemic SMN protein restoration also rescued *Smn*$^{2B/-}$ mice more robustly than an intracerebroventricular (ICV) delivery route, while intravenous (IV) administration was enough to rescue phenotypic, neuromuscular junction (NMJ) and peripheral tissue pathology without rescue of the motor neurons.[18,19] Of note, numerous pathologies of the liver, including decreased IGF1 levels and steatosis, were rescued by systemic treatment, likely contributing to the increased survival of both Taiwanese and *Smn*$^{2B/-}$ mice.[18–20]

The extra-neuronal component of SMA is also documented in human patients; in fact, in 1999 reports of abnormal fatty acid metabolism led to a large cohort study on fatty acids in patients with SMA.[21] This work demonstrated the presence of abnormal dicarboxylic aciduria and increased levels of dodecanoic acid in plasma independent of muscle denervation.[21] More

recently, clinical reports from a large cohort of paediatric SMA type I-III patients as well as SMA type I liver necropsy data identified an increased susceptibility to developing dyslipidaemia and liver steatosis.[22] Evidence of liver abnormalities comes from non-invasive imaging on and serum from human patients with SMA, while necropsies of paediatric patients with SMA display hepatic microvesicular steatosis.[23] Furthermore, metabolic abnormalities are seen across paediatric neuromuscular disorders beyond SMA, including Duchenne muscular dystrophy, with increased risk of liver enlargement, steatosis and fibrosis.[24] Liver pathology across these diseases resemble that of metabolic dysfunction-associated steatotic liver disease (MASLD), the hepatic manifestation of metabolic syndrome, demonstrating an increased risk for an altered liver metabolome and liver involvement in disease pathophysiology.[24]

Since SMA is a multi-system disease, patients now surviving into adulthood, as a result of the approved therapies, may experience significant comorbidities from untreated peripheral pathologies.[25] The peripheral requirement of SMN protein in each tissue and how this contributes to motor neuron function and dysfunction is yet to be uncovered.[25] As liver pathology is becoming increasingly reported and affirmed as a contributor to SMA pathology, we set out to determine the greater impact of liver pathology on the rest of the body.

Methods

Animals

Mice were housed at the University of Ottawa Animal Care Facility. Food and water was available ad libitum for all cages, housing conditions remained constant across all experimental cages. A total of 78 mice were used in this study. $Smn^{2B/-}$ mice were developed in house by the Kothary laboratory.[16] The $Smn^{2B/-}$ mouse line was produced by breeding $Smn^{+/-}$ mice (C57BL/6J background, RRID:IMSR_JAX:006214) with $Smn^{2B/2B}$ mice (C57BL/6J background, RRID:IMSR_JAX:034285).[26] This genetic cross produces offspring of $Smn^{2B/-}$ and $Smn^{2B/+}$ mice. $Smn^{2B/-}$ phenotypically present with SMA like neurological defects while $Smn^{2B/+}$ are the healthy littermates used as controls. $Smn^{2B/-}$ and $Smn^{2B/+}$ mice were of similar age and gender, of note, $Smn^{2B/-}$ mice are of lower weight than $Smn^{2B/+}$ littermates as the $Smn^{2B/-}$ mice suffer from the SMA-like disease state. The SMNΔ7 mouse line (FVB background, RRID:IMSR_JAX:005025) was used to see if liver-specific SMN restoration impacted pathology in a severe model of SMA. Δ7 heterozygotes ($Smn^{+/-}$;$SMN2^{+/+}$;$SMN\Delta7^{+/+}$) were crossed to generate Δ7 SMA ($Smn^{-/-}$;$SMN2^{+/+}$;$SMN\Delta7^{+/+}$) mice. Δ7 SMA mice develop symptoms ~ P4 and survive 13 days without treatment.

AAV9-albumin-SMN protein treatment

The adeno-associated viral vector serotype 9 (AAV9)-albumin-SMN vector was produced in HEKExpress™ cells adapted to suspension, as described in.[27] The titer of AAV9 suspension measured by dPCR was 1.52×10^{13} viral genomes (vg)/mL. The AAV9 carries the human *SMN1* gene controlled by an albumin gene promoter, driving liver specific transgene expression.[28] Mice were administered AAV9-albumin-SMN on P1 via ICV injection at a dose of 1.8×10^{11} vg/pup, in $Smn^{2B/-}$ mice, and 3×10^{10} vg/pup in Δ7 mice, in a volume of 3 µl. Mice administered AAV9-cba-SMN at P1 via ICV injection received 5×10^{10} vg/pup. Facial IV injections were administered at a dose of 1.5×10^{11} vg/pup. Cages were housed in containment facility level two at University of Ottawa Animal Care Facility for 72 h after injection, after which they were transferred back to general housing for the remainder of use. Two litters from treated and untreated mice were monitored for weight, motor function and survival and sacrificed at P65. Weight and survival were assessed on untreated mice until humane endpoint, defined as 4 days consecutive weight loss or 20% overall weight loss. Mice were weighed every two days until sacrifice and tissue collection at P65. Tissues were collected from additional untreated mice at P19. An additional litter underwent rotarod assessment and survival until humane endpoint. Blinding of treatment conditions during rotarod assessment was not possible due to only treated animals being able to perform the test.

Motor function test

Rotarod tests assessed neuromuscular coordination and balance. Rotarod performance was conducted at the University of Ottawa, Faculty of Medicine Animal Behaviour and Physiology Core. Treated $Smn^{2B/-}$ and control $Smn^{2B/+}$ mice were subjected to the rotarod once every two weeks from P21 until humane endpoint. Each test consisted of 4 trials of 4–45 rpm, accelerating ramp over 300 s with an inter-trial interval of 1 min. Motor function of Δ7 SMA mice and littermate controls was assessed by the righting reflex test, during this assessment the mouse is placed on its back and the time it takes the mouse to right itself is recorded. Righting reflex was assessed every two days from P5.

Blood collection and plasma analysis

Mice were euthanised by decapitation after asphyxiation in a CO_2 chamber. Upon decapitation, Microcuvette CB 300 K2E tubes (Sarstedt, Newton, NC) coated with K2 EDTA were used to collect one blood sample per mouse. Blood was centrifuged at room temperature, 5000 rcf for 5 min using 5242R centrifuge (Eppendorf). Supernatant was collected and stored at –80 °C. A neurofilament (NfL) assay was performed and concentration of NfL protein was determined using the Quanterix's Simoa® NfLight™ Advantage Kit (Qanterix, Catalog No: 103186), run as a batched assay and as per manufacturer's instructions by Eastern Ontario Regional Laboratory Association (EORLA), at the Ottawa Hospital

General Campus. Plasma IGF-1 levels were also determined using an IGF1 enzyme-linked immunosorbent assay (ELISA), Mouse/Rat IGF-1 ELISA kit (R&D systems, Minneapolis, MN, USA; Catalog No: MG100).

Immunoblotting

After euthanasia at either P9, P19 or P65, tissues (spinal cord, liver, *tibialis anterior* (TA) muscle) were flash frozen in Microvette CB 300 Z tubes (Sarstedt) in liquid nitrogen and stored at –80 °C. Total protein lysate was collected from tissues that were homogenised using a PowerGen 125 homogeniser, 7 × 95MM generator (Fisher Scientific, Massachusetts, US) in radioimmunoprecipitation assay (RIPA) lysis buffer and phenylmethylsulfonyl fluoride (PMSF) (Cell Signalling, Danvers, MA). Protein concentrations were determined by Bicinchoninic Acid assay (BCA) assay (ThermoFisher, CA). Twenty µg of protein was loaded onto a 12% polyacrylamide gel and subjected to gel electrophoresis and examined by immunoblot. The proteins were then transferred to a PVDF membrane (Immobilon-FL, Millipore, Burlington, MA) and blocked at room temperature for 1 h in Odyssey blocking buffer (LI-Cor, Lincoln, NE) or 5% milk (chemiluminescence), modified from previously described methods.[29] Signals were detected using the Odyssey (LI-COR) imager or by enhanced chemiluminescence (Pierce), with α-tubulin used as the housekeeping control (Supplemental Table S1). Results were normalised to α-tubulin.

RT-qPCR

RNA was extracted from liver using the RNeasy Mini Kit, Qiagen (Hilden, Germany). Reverse transcription was performed using RT^2 first kit according to manufacturer's instructions. Each reaction contained equal amounts of cDNA, RNase free water, Evagreen SyBR (Bio-Rad, Hercules, CA) and primers (100 nmol/L) in a final volume of 20 µl. A standard curve was performed for each primer set to ensure efficiency. To confirm amplicon specificity, a melting curve analysis was performed. Negative controls for each primer were included in each PCR plate, containing water instead of cDNA. The RT-qPCR was analysed using $^{\Delta\Delta ct}$ or $^{\Delta ct}$ methods. Results were normalised to housekeeping gene *Actb* (Supplemental Table S1).

Tissue processing and staining

Haematoxylin and Eosin stain

After euthanasia at either P19 or P65, liver, pancreas and TA muscle (one per mouse) were washed in phosphate buffered saline (PBS) and fixed in 4% paraformaldehyde (PFA) for 24 h at 4 °C, then transferred to 70% ethanol before processing. The University of Ottawa Pathology and Laboratory Medicine Department processed the liver, pancreas and TA, embedding the tissues in wax using a LOGOS microwave hybrid tissue processor (Milestone Medical, Kalamazoo, MI). The paraffin block tissues were sectioned with a microtome at 3–4 µm thickness. Haematoxylin and Eosin (H&E) staining was performed on liver and TA sections using an XL CV5030 autostainer (Leica, Wetzlar, Germany). H&E stained slides were then scanned with MIRAX MIDI digital slide scanner (Zeiss, Oberkochen, Germany) and images were acquired using the panoramic viewer 1.15.4 (3DHISTECH, Budapest, Hungary). Liver steatosis was visualised and muscle myofiber area was measured using ImageJ (version 1.53K).

Insulin/glucagon pancreas stain

Pancreas sections were deparaffinised by 3 washes of 5 min in xylene substitute HistoClear (National Diagnostics, Atlanta,GA). Sections were washed in 50:50 HistoClear:absolute ethanol for 5 min. Slides were gradually rehydrated in 100%, 95%, 70%, 50% ethanol followed by water. To begin staining, slides were incubated in 0.5% Triton-X 100 (Millipore, Sigma, Burlington, MA) in PBS for 5 min. Slides were washed 3x with PBS and blocked in 0.3% Triton-X-100, 20% goat serum in tris-buffered saline (TBS) for 2 h. Primary antibodies for insulin (1:50) and glucagon (1:200) were diluted in 0.3% Triton-X-100, 2% goat serum in TBS and slides were incubated at 4 °C overnight (Supplementary Table S1). Slides were washed 3 × 10 min in PBS and incubated in secondary antibodies in 0.3% Triton-X-100, 2% goat serum in TBS for 1 h (Supplementary Table S1), followed by additional 3 × 10 min PBS washes. Slides were incubated in DAPI (1:1000) and mounted in DAKO mounting medium (Agilent, Santa Clara, CA). Images were taken at 20x with a fluorescence Axio Imager M2 microscope (Zeiss), insulin and glucagon positive cells were counted using ImageJ.

Oil-Red-O stain

Frozen tissue was placed in a cryomold OCT block and sectioned at 10 µm. The University of Ottawa Pathology and Laboratory Medicine Department stained the liver slides in Oil-Red-O. Stained slides were scanned using an AxioCam 305 colour camera (Zeiss). Liver lipid droplet accumulation was visualised by red stain intensity.

Choline acetyltransferase (ChAT)

The lumbar spinal cord was fixed in 4% PFA for 24 h at 4 °C, transferred to 30% sucrose solution before being placed in OCT cryomolds. Spinal cords were section and stained for ChAT (1:100) as previously described.[30] The number of ChAT positive motor neuron cell bodies were counted per ventral horn, 5 sections separated by 100 µm, per animal.

Neuromuscular junction stain

The abdominal musculature was dissected and fixed in 4% PFA for 15 min, followed by three washes of 10 min in PBS. The transverse abdominus (TVA) muscle was

later dissected away from the rib and other abdominal muscles as previously described.[31] TVA NMJs were stained by α-bungarotoxin (BTX, 1:1000), NF (NF, 1:100) and synaptic vesical protein (SV2, 1:250). Briefly, the TVA was incubated with tetramethyl rhodamine (TRITC) conjugated bungarotoxin for 30 min at room temperature. Next the sections were incubated with primary antibodies for NF and SV2 overnight at 4 °C (Supplementary Table S1). Tissues were mounted with DAKO mounting medium (Agilent) and Z-stack images were taken using a fluorescent Axio imager M2 microscope (Zeiss) at 20x. ImageJ was used to count NMJs with neurofilament accumulation and end plate occupancy.

Transmission electron microscopy

Electron microscopy (EM) was performed as previously described.[32] Briefly, untreated P19 and AAV9-albumin-SMN treated P65 $Smn^{2B/-}$ mice as well as P65 untreated and treated $Smn^{2B/+}$ mice were anesthetised and then perfused transcardially with 5 mL PBS, followed by 10–20 mL Karnovsky's fixative (4% PFA, 2% glutaraldehyde, and 0.1 mol/L sodium cacodylate in PBS, pH7.4). Livers were dissected and fixed overnight at 4 °C, and a 1–2 mm segment of liver tissue was collected from the same lobe of each mouse and processed for EM. All samples were observed under a transmission EM (Hitachi 7100, Gatan digital camera; Tokyo, Japan) operated at 75 kV. Images were for qualitative purposes only.

Statistical analyses

Data are presented as the mean ± standard error of the mean. Statistical tests were performed using GraphPad Prism 10.2. Data normality tests were performed using a Gaussian distribution test, Shapiro–Wilk test (alpha 0.05). Q–Q plots were graphed to assess normality. Parametric unpaired t-tests, one-way ANOVA with Tukey's post-hoc test or two-way ANOVA with Bonferroni's post-hoc tests were performed. Kaplan–Meier survival analysis was performed using the log-rank (Mantel–Cox) test, survival curves were considered significantly different at $P < 0.05$. Statistical significance is indicated by number of asterisks; *$P \leq 0.05$, **$P \leq 0.01$, ***$P \leq 0.001$, ****$P \leq 0.0001$. Outliers were determined using Grubbs' test, GraphPad calculator. Grubbs' test was performed on all data sets, individually, to determine whether the most extreme value in the list was a significant outlier from the rest. If this was the case, outliers were excluded from the analysis. Significance level was set to alpha 0.05. Mice were randomly assigned to treatment groups, regardless of sex, and images were blinded prior to quantification. To determine any sex differences additional subgroup analysis was performed on phenotypic data sorted by sex. N numbers given refer to single animals ranging from N-of-3 to N-of-14 per experiment. Sample size was determined by a resource equation approach (E = total number of animals-total number of groups). In this study E falls between 13 and 16 ($Smn^{2B/-}$ treated (N = 8) vs. untreated (N = 7) E = 13, $Smn^{2B/+}$ treated (N = 8) vs. untreated (N = 10) E = 16), where E10-20 can be considered as an adequate sample size. Where sample size was lower than n = 5, distribution was considered normal, as sample size is too small to perform a robust distribution test.

Ethics

Animals were cared for according to the Canadian Council on Animal Care and all experiments were performed in accordance with ARRIVE guidelines and approved by the University of Ottawa Animal Care Committee (protocol: OHRIe-3709).

Role of funding source

The funding agencies of this study did not influence the study design, data collection, analysis, interpretation of data, or manuscript preparation.

Results

Intracerebroventricular and intravenous injection of AAV9-albumin-SMN successfully increases observed SMN protein quantity in the liver alone in $Smn^{2B/-}$ mice

We injected our liver-specific viral vector (AAV9-albumin-SMN) at P1 via ICV injection (Fig. 1). We have previously shown ICV delivery of AAV9-SMN can cross the blood brain barrier (BBB) and distribute peripherally, making it an efficient delivery route.[19] Since the albumin promoter has been demonstrated to drive transgene expression only in the liver, we initially confirmed the liver-specific expression of SMN protein by RT-qPCR and immunoblot.[28,33,34] We extracted RNA from liver, brain, spinal cord and muscle at P19 and P65 and performed sensitive RT-qPCR analysis to specifically detect human *SMN1* mRNA that might be present in the AAV9-albumin-SMN treated samples (Fig. 2a and b). *SMN1* mRNA levels were not dissimilar to *SMN1* levels in AAV9-cba-SMN treated $Smn^{2B/-}$ spinal cord controls at both P19 and P65 (Fig. 2a and b). *SMN1* transcript levels were not detected in brain, spinal cord and muscle from AAV9-albumin-SMN treated mice compared to AAV9-cba-SMN treated $Smn^{2B/-}$ spinal cord controls at both P19 and P65 (Fig. 2a and b).

Next, we extracted protein from liver at early and late time points (P9 and P65), spinal cord and muscle (P65) and performed immunoblot analysis using a pan-SMN (SMN) antibody to detect both mouse and human SMN. We demonstrate 78.4% of SMN is present in the liver of ICV treated P65 $Smn^{2B/-}$ mice compared to treated $Smn^{2B/-}$ spinal cord (2.1%) and muscle (19.4%) (Fig. 2c). SMN expression is significantly increased in P9 livers

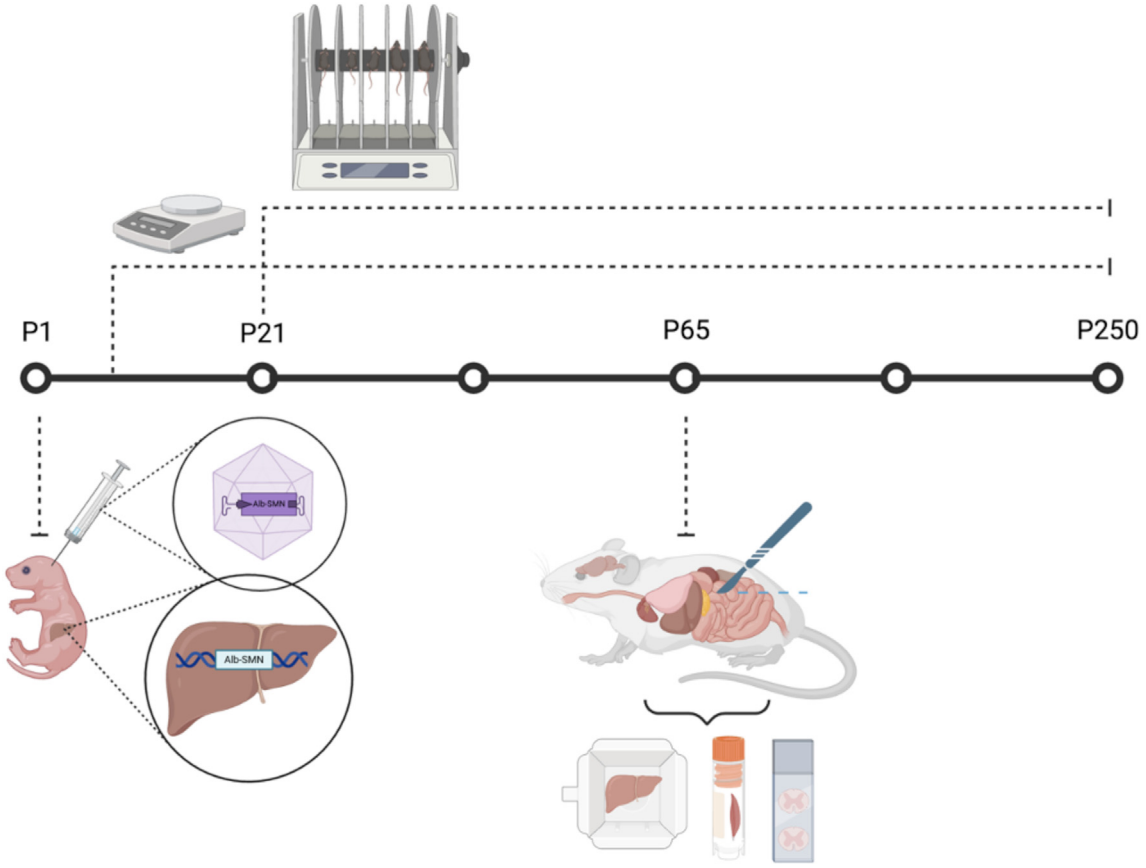

***Fig. 1:* Study design,** schematic representation of the experimental design and time points of phenotypic data and tissue collections. Injections were performed at P1, mice were phenotypically monitored for weight, motor function and survival until humane endpoints were reached. Weight was taken every 2 days starting at P0, motor function was assessed starting at P21. Tissues were collected at P9, P19 and P65. Schematic created with BioRender.com.

from AAV9-albumin-SMN treated $Smn^{2B/-}$ ($P = 0.0002$) and $Smn^{2B/+}$ mice ($P < 0.0001$) (Supplemental Figure S1). We demonstrate higher expression of SMN protein at an earlier timepoint in the livers of treated $Smn^{2B/-}$ mice, likely due to a substantial change in postnatal requirement for SMN protein expression (Fig. 2d and Supplemental Figure S1).[35] SMN expression is also not significantly different in P65 livers from AAV9-albumin-SMN treated $Smn^{2B/-}$ mice compared to untreated $Smn^{2B/+}$ controls ($P = 0.4511$) (Fig. 2e). There is minimal expression of SMN protein in the spinal cord or the muscle of $Smn^{2B/-}$ treated mice (Fig. 2f–i).

Similarly, liver specific SMN expression is significantly increased in IV AAV9-albumin-SMN treated P9 $Smn^{2B/-}$ mice compared to vehicle treated $Smn^{2B/-}$ mice ($P = 0.0002$) (Supplemental Figure S2a and b). SMN levels remain the same in spinal cord and skeletal muscle from P9 AAV9-albumin-SMN treated compared to vehicle treated $Smn^{2B/-}$ mice (Supplemental Figure S2c–f). We demonstrate 78.4% of SMN is present in the liver of IV treated P9 $Smn^{2B/-}$ mice compared to treated $Smn^{2B/-}$ spinal cord (5.5%) and muscle (16%) (Supplemental Figure S2g).

Following confirmation of liver-specific SMN protein expression post AAV9-albumin-SMN treatment, we decided to investigate human-SMN (hSMN) to identify the human-specific protein produced by AAV9 delivery of the human *SMN1* gene to the liver. Immunoblot using a human-specific SMN protein antibody similarly demonstrated expression of hSMN protein restricted to the liver with no detectable protein in the spinal cord or muscle (lower panels in Fig. 2d–f,h). Notably, we saw no AAV9-mediated hSMN protein expression in the livers of injected $Smn^{2B/+}$ mice at P65, loss of transgene expression in other studies has been attributed to hepatocyte turnover, thus could explain this finding (Fig. 2d).[36] These results indicate SMN protein delivery under an albumin promoter can successfully increase SMN protein expression in the liver, with no detection of SMN protein in additional CNS or peripheral tissues.

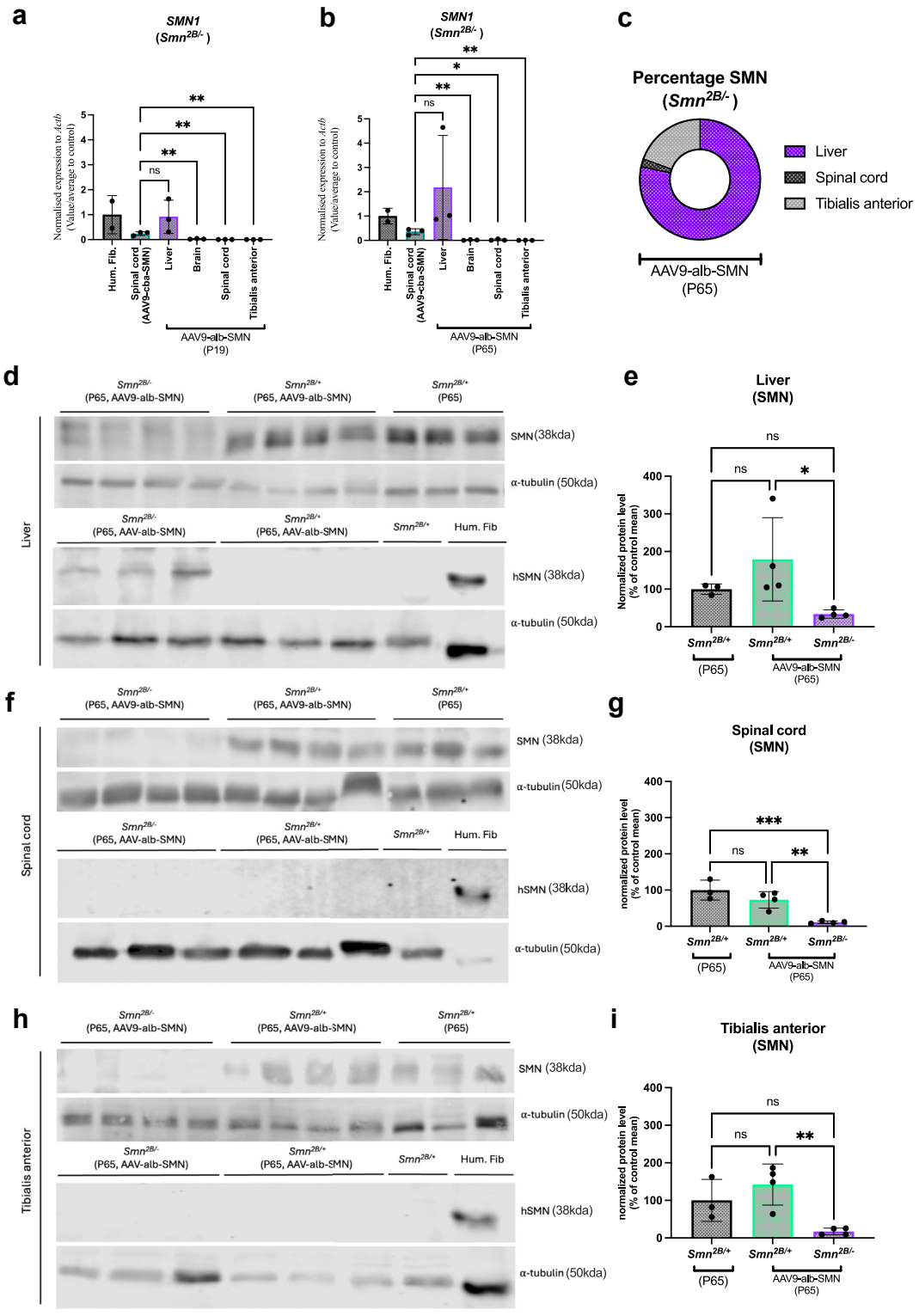

Fig. 2: **Liver specific SMN mRNA and protein expression following AAV9-albumin-SMN ICV injections, a.** RT-qPCR of SMN mRNA expression in P19 liver, brain, spinal cord and muscle following AAV9-albumin-SMN treatment compared to AAV9-cba-SMN P19 spinal cord, human fibroblast cell line SMN control, **b**. RT-qPCR of SMN mRNA expression in P65 liver, brain spinal cord and muscle following AAV9-

Weight, neuromuscular coordination and survival are increased in *Smn*$^{2B/-}$ mice following AAV9-albumin-SMN treatment

To evaluate the impact of liver health on SMA pathophysiology, we conducted phenotypic analysis on AAV9-albumin-SMN treated and untreated mice. Weight, neuromuscular coordination, and survival were assessed through to a humane endpoint (Fig. 3). All mice were monitored every two days for weight and every two weeks for neuromuscular coordination and balance using the rotarod apparatus. AAV9-albumin-SMN treatment significantly increased the weight of *Smn*$^{2B/-}$ mice compared to untreated mice ($P < 0.0001$), however weight was never rescued to that of the healthy control littermates (Fig. 3a and b). IV administration of AAV9-albumin-SMN did not change the weight of *Smn*$^{2B/-}$ mice between P5–P20 compared to vehicle treated *Smn*$^{2B/-}$ mice (Supplemental Figure S2h). Untreated *Smn*$^{2B/-}$ mice had a median survival of 20 days and could not perform the rotarod test after this age, though it is expected that they would perform poorly given their moribund state. For this reason, neuromuscular coordination assessment was conducted on treated *Smn*$^{2B/-}$ mice and compared against their healthy littermates (*Smn*$^{2B/+}$). Time spent on the rotarod was not significantly different between treated *Smn*$^{2B/-}$ mice and their healthy littermates (*Smn*$^{2B/+}$) at P65 ($P = 0.2079$) (Fig. 3c). After P100 treated *Smn*$^{2B/-}$ mice showed a steady decline in their neuromuscular coordination ability and a significant reduction in time spent on the rotarod was seen beyond this time point between treated *Smn*$^{2B/-}$ mice and their healthy littermates ((*Smn*$^{2B/+}$) ($P < 0.05$) Fig. 3d).

Next, we assessed survival and found a significant increase in lifespan between untreated *Smn*$^{2B/-}$ mice and treated *Smn*$^{2B/-}$ mice following ICV administration ($P < 0.0001$) (Fig. 3e, Supplemental Figure S2i). We continued our survival analyses until mice reached their humane endpoints, survival proportion between treated *Smn*$^{2B/-}$ mice and their healthy littermates (*Smn*$^{2B/+}$) was not dissimilar up until P100. Survival of treated *Smn*$^{2B/-}$ mice gradually declined beyond P100 and there was a significant difference compared to their healthy littermates (*Smn*$^{2B/+}$) at an older age ($P = 0.0383$) (Fig. 3f). Interestingly, we did notice a difference in response to treatment between male and female *Smn*$^{2B/-}$ mice (Supplemental Figure S3). As expected, male mice weighed significantly more than female mice ($P < 0.001$), however neuromuscular coordination, and balance in treated *Smn*$^{2B/-}$ female mice was significantly better than *Smn*$^{2B/-}$ male littermates ($P < 0.001$) (Supplemental Figure S3a–d). While female *Smn*$^{2B/-}$ mice did live longer than *Smn*$^{2B/-}$ male littermates, there was not a significant difference between the sexes ($P = 0.1966$) (Supplemental Figure S3e and f). Taken together, liver-specific SMN protein restoration alone was enough to significantly improve the survival of *Smn*$^{2B/-}$ mice. This highlights the importance of liver intrinsic SMN protein to overall health.

Following a significant increase in survival of the *Smn*$^{2B/-}$ mice as a result of AAV9-albumin-SMN treatment, we decided to investigate whether treatment would have the same impact in a severe *Smn*$^{-/-}$;SMN2; Δ7 mouse model of SMA (Supplemental Figure S4a). We did not see a significant improvement in survival or weight of treated Δ7 mice compared to untreated Δ7 mice ($P = 0.0701$) (Supplemental Figure S4b and c). However, a small, but significant improvement in the ability to right was seen (P5–P12) in *Smn*$^{-/-}$;SMN2; Δ7 mice following AAV9-albumin-SMN treatment ($P < 0.05$) (Supplemental Figure S4d). Notably, this experiment was only performed on one Δ7 litter, using a low dose of viral vector (available at the time of experiment).

Fatty liver phenotype is rescued and liver function, triglyceride levels and IGF-1 expression are restored following AAV9-albumin-SMN treatment in *Smn*$^{2B/-}$ mice

The main organ of interest in our study was the liver, specifically the fatty liver phenotype reported in *Smn*$^{2B/-}$ mice.[15] We assessed the fatty liver by three methods: H&E stain, EM and Oil-Red-O stain. The use of H&E staining enabled visualisation of microvesicular steatosis, while EM and Oil-Red-O show lipid accumulation. Untreated *Smn*$^{2B/-}$ mice display significant steatosis and lipid droplet accumulation, while treatment with AAV9-albumin-SMN (both ICV and IV administration)

albumin-SMN treatment compared to AAV9-cba-SMN P19 spinal cord, human fibroblast cell line SMNA control, **c**. percentage protein expression in liver, spinal cord and muscle from P65 *Smn*$^{2B/-}$ AAV9-albumin-SMN treated mice, demonstrative donut chart, **d.** Western blots of SMN using a pan-active antibody (SMN) or a human-specific antibody (hSMN) in P65 liver following AAV9-albumin-SMN treatment in P65 *Smn*$^{2B/-}$, *Smn*$^{2B/+}$ mice with untreated *Smn*$^{2B/+}$ and human fibroblast controls (hSMN blot), **e.** Liver SMN expression Western blot quantification of AAV9-albumin-SMN treatment in P65 *Smn*$^{2B/-}$, *Smn*$^{2B/+}$ mice with untreated *Smn*$^{2B/+}$, **f.** Western blots of SMN and hSMN protein expression in spinal cord following AAV9-albumin-SMN treatment in P65 *Smn*$^{2B/-}$, *Smn*$^{2B/+}$ mice with untreated *Smn*$^{2B/+}$ and human fibroblast controls, **g.** Spinal cord SMN expression Western blot quantification of AAV9-albumin-SMN treatment in P65 *Smn*$^{2B/-}$, *Smn*$^{2B/+}$ mice with untreated *Smn*$^{2B/+}$, **h.** Western blots of SMN and hSMN protein expression in tibialis anterior muscle following AAV9-albumin-SMN treatment in P65 *Smn*$^{2B/-}$, *Smn*$^{2B/+}$ mice with untreated *Smn*$^{2B/+}$ and human fibroblast controls, **i.** Tibialis anterior muscle SMN expression Western blot quantification of AAV9-albumin-SMN treatment in P65 *Smn*$^{2B/-}$, *Smn*$^{2B/+}$ mice with untreated *Smn*$^{2B/+}$. Note that a pan SMN antibody was used in the analysis (treated *Smn*$^{2B/-}$ N = 4, treated *Smn*$^{2B/+}$ N = 4, untreated *Smn*$^{2B/+}$ N = 3) (T-test, one-way ANOVA, *≤0.01, **P ≤ 0.01, ***P ≤ 0.001, ns = non-significant).

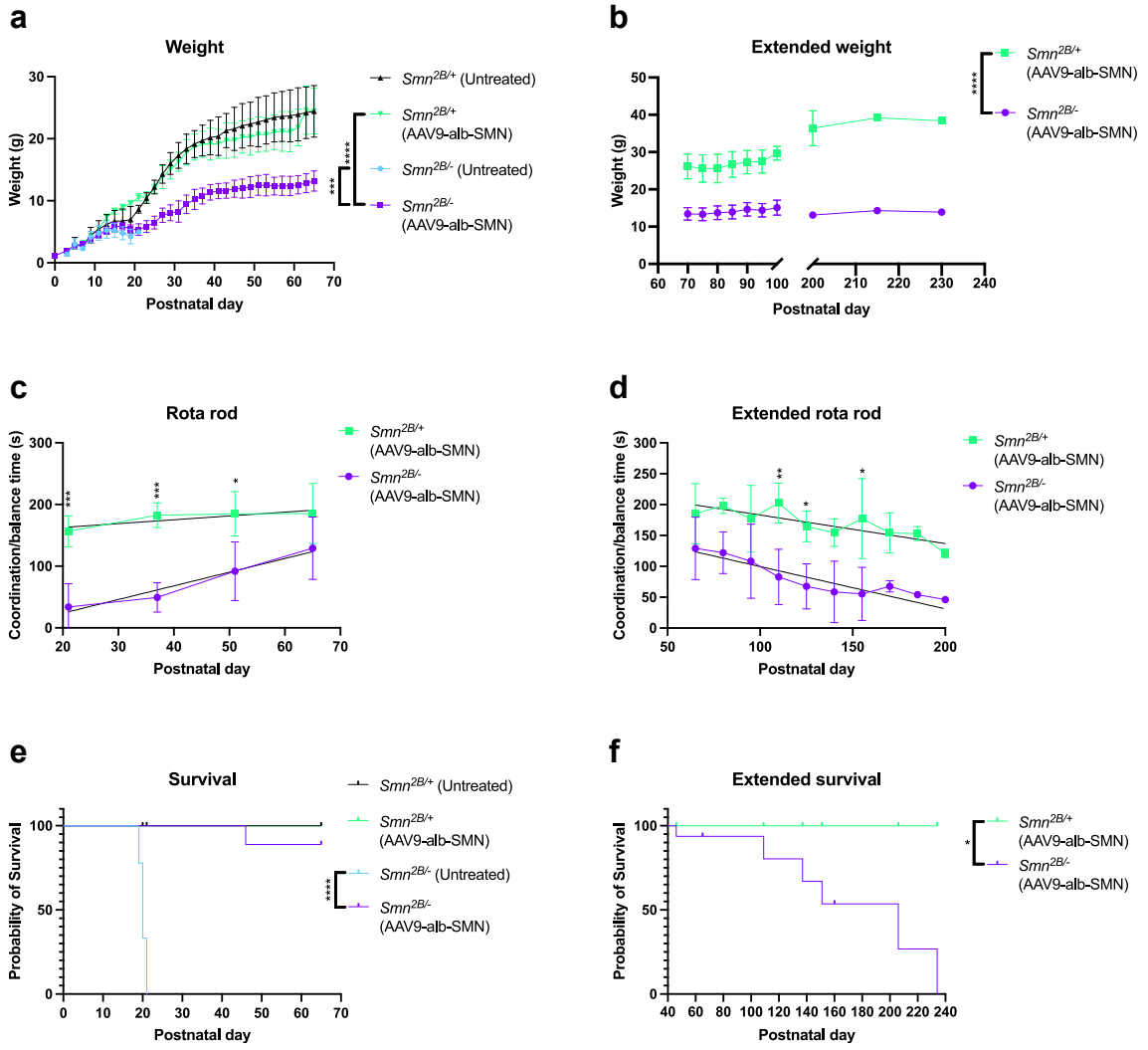

Fig. 3: **Phenotypic analysis of weight, neuromuscular coordination and survival of *Smn*$^{2B/-}$ mice following ICV injection of AAV9-albumin-SMN, a.** Weight of treated and untreated *Smn*$^{2B/-}$ and *Smn*$^{2B/+}$ mice from P0 to P65, **b.** Weight of treated *Smn*$^{2B/-}$ and *Smn*$^{2B/+}$ mice from P65 to P240, **c.** Rotarod assessment of treated and untreated *Smn*$^{2B/-}$ and *Smn*$^{2B/+}$ mice from P0 to P65, **d.** Rotarod assessment of treated *Smn*$^{2B/-}$ and *Smn*$^{2B/+}$ mice from P65 to P200, **e.** Survival Kaplan–Meier curve of treated and untreated *Smn*$^{2B/-}$ and *Smn*$^{2B/+}$ mice from P0 to P65, **f.** Survival Kaplan–Meier curve of treated *Smn*$^{2B/-}$ and *Smn*$^{2B/+}$ mice from P65 to P240. Two litters from treated (*Smn*$^{2B/-}$ N = 8, *Smn*$^{2B/+}$ N = 8) and untreated (*Smn*$^{2B/-}$ N = 7, *Smn*$^{2B/+}$ N = 10). Weight was monitored every two days from P0 and every week from P65, rotarod assessments were conducted every two weeks from P21 (Two-way ANOVA, Kaplan–Meier survival analysis, *P ≤ 0.05, ***P ≤ 0.001, ****P ≤ 0.0001).

rescued the fatty liver phenotype and prevented lipid accumulation in the liver (Fig. 4a and b and Supplemental Figure S2k). Notably, P65 treated *Smn*$^{2B/-}$ livers have a residual pink hue suggesting that although the fatty liver is rescued, it is not complete. Nevertheless, detailed EM images display the reduction in lipid droplets between untreated and treated *Smn*$^{2B/-}$ mice (Fig. 4a).

Additionally, we confirmed that triglyceride levels were significantly increased in untreated P19 *Smn*$^{2B/-}$ mice (P < 0.001) (Fig. 4c). Triglyceride levels were restored to normal in treated P65 *Smn*$^{2B/-}$ mice with levels similar to that of controls (Fig. 4c). As we found a rescue of liver steatosis, we continued to investigate the impact of intrinsic SMN protein on liver function. We have previously reported liver function defects present in the *Smn*$^{2B/-}$ mouse model.[15] Specifically, untreated *Smn*$^{2B/-}$ mice have depletion of IGF-1 protein in plasma.[15,22] Plasma IGF-1 protein levels were confirmed to be significantly increased in treated P65 *Smn*$^{2B/-}$ mice compared to untreated P19 *Smn*$^{2B/-}$ mice (P = 0.0003) and were restored to that of healthy controls in P65 mice (P = 0.0597) (Fig. 4d).

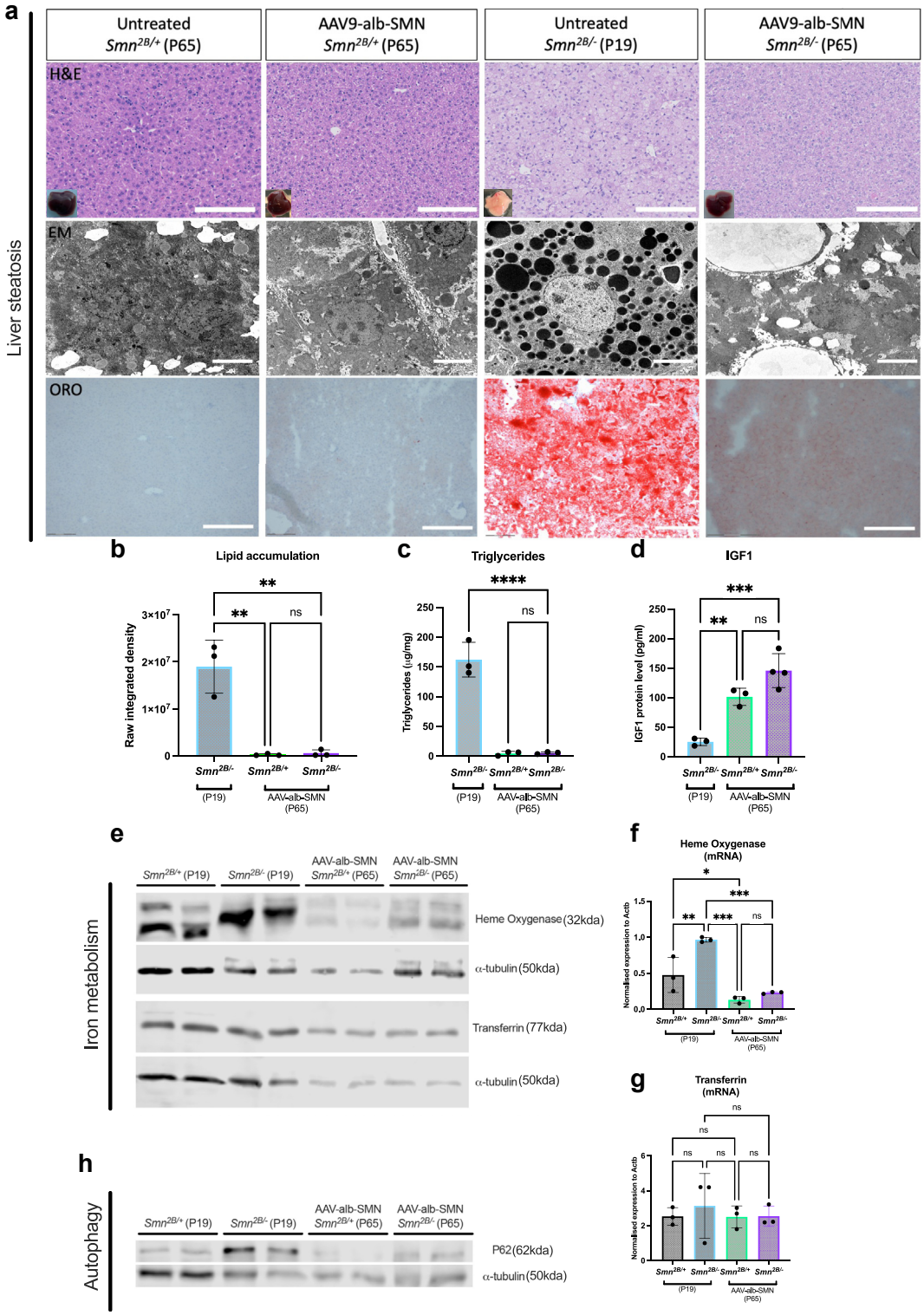

Fig. 4: **Fatty liver is rescued and liver functions are restored following AAV9-albumin-SMN ICV injection, a.** Representative H&E-stained liver sections (scale bar 100 µm), electron microscopy images of lipid droplets (qualitative purposes only N = 1 per group, scale bar 5 µm), and Oil-Red-O stained liver sections from treated P65 *Smn*$^{2B/-}$ *mice,* treated P65 *Smn*$^{2B/+}$ mice, untreated P19 *Smn*$^{2B/-}$ mice and untreated P65 *Smn*$^{2B/+}$ mice with inset photographs of liver appearance upon dissection (scale bar 150 µm), **b.** quantification of lipid droplet accumulation

In line with these findings, we have previously reported differential protein expression of key iron metabolism markers; heme oxygenase (HO-1) is increased in untreated *Smn*$^{2B/-}$ mice while transferrin levels remain similar to healthy controls.[15,22] Here, we confirmed these findings by Western blot whereby HO-1 was significantly increased in untreated *Smn*$^{2B/-}$ mice and demonstrate a rescue following ICV AAV-albumin-SMN treatment (Fig. 4e). HO-1 mRNA transcripts were also reduced in both *Smn*$^{2B/-}$ and *Smn*$^{2B/+}$ treated mice at P65 ($P < 0.001$) (Fig. 4f). Due to enhanced oxidative stress, accompanied by compensatory induction of HO-1, during aging, it is possible treatment also accounts for the reduction in *Smn*$^{2B/+}$ mice.[37,38] IV AAV9-albumin-SMN administration did not significantly change HO-1 or transferrin protein levels in *Smn*$^{2B/-}$ mice compared to untreated *Smn*$^{2B/-}$ mice, P62 levels were significantly reduced in IV treated *Smn*$^{2B/-}$ mice ($P < 0.0001$) (Supplemental Figure S2l–p). Transferrin protein and mRNA levels remained similar to healthy controls (Fig. 4e–g). Additionally, we have also previously reported autophagy marker P62 to be in increased in untreated *Smn*$^{2B/-}$ mice.[15,22] Here, we see a trend towards increased P62 protein levels in untreated *Smn*$^{2B/-}$ mice, reduced following ICV AAV9-albumin-SMN treatment (Fig. 4h).

AAV9-albumin-SMN treatment does not rescue spinal cord motor neuron degeneration but does result in a decrease in neurofilament protein in the plasma at P65

To determine whether liver SMN protein restoration has an impact on CNS pathologies, we analysed motor neuron cell body counts and plasma NfL levels. We confirmed the loss of motor neuron cell bodies, a hallmark pathology of SMA, in our untreated P19 *Smn*$^{2B/-}$ mice ($P = 0.0327$) (Fig. 5a and b).[39] Motor neuron counts from P65 treated *Smn*$^{2B/-}$ mice remained significantly reduced compared to healthy controls, therefore AAV9-albumin-SMN treatment did not protect against motor neuron loss ($P = 0.0276$) (Fig. 5c). In addition to monitoring motor neuron count, we also assessed NfL levels that are normally elevated in untreated *Smn*$^{2B/-}$ mice at P19 ($P < 0.0001$) (Fig. 5d). Nfl levels remain elevated in both ICV and IV AAV9-albumin-SMN treated P19 *Smn*$^{2B/-}$ mice ($P > 0.05$) (Supplemental Figure S2j). Interestingly, we observed a reduction in NfL levels at P65 possibly demonstrating a developmental reduction in Nfl as the mice age. NfL levels were restored back to levels of healthy controls in P65 *Smn*$^{2B/-}$ mice ($P = 0.7564$) (Fig. 5e).

AAV9-albumin-SMN treatment rescues neuromuscular junction pathology in *Smn*$^{2B/-}$ mice

Next, we analysed the impact of AAV9-albumin-SMN treatment on NMJ pathology. It is well documented that *Smn*$^{2B/-}$ mice exhibit reduced endplate occupancy and increased neurofilament accumulation at the NMJ.[40] For this reason, we assessed percentage endplate occupancy and neurofilament accumulation in *Smn*$^{2B/-}$ mice and control littermates (Fig. 6a). As expected, we found the percentage of endplates occupied by a motor neuron was significantly reduced in untreated P19 *Smn*$^{2B/-}$ mice compared to untreated P19 *Smn*$^{2B/+}$ mice ($P = 0.0023$) (Fig. 6b). Percentage NMJ occupancy of treated P65 *Smn*$^{2B/-}$ mice was significantly reduced compared to untreated P65 *Smn*$^{2B/+}$ mice ($P = 0.0056$) (Fig. 6c). NMJ occupancy was similar between treated *Smn*$^{2B/-}$ and treated *Smn*$^{2B/+}$ mice at P65 ($P = 0.5198$) (Fig. 6c). Neurofilament accumulation was significantly increased in P19 untreated *Smn*$^{2B/-}$ mice compared to in untreated P19 *Smn*$^{2B/+}$ mice ($P < 0.0001$) (Fig. 6d). Neurofilament accumulation in treated *Smn*$^{2B/-}$ mice was increased compared to *Smn*$^{2B/+}$ controls at P65 ($P = 0.0391$) (Fig. 6e). Overall, although NMJ pathology is modestly rescued in treated *Smn*$^{2B/-}$ mice, it does not reach that of healthy control littermates. This result is consistent with our other biochemical observations on motor neuron counts (Fig. 5) and functional data (Fig. 3).

Myofiber area size but not centralised nucleation is rescued in *Smn*$^{2B/-}$ mice following AAV9-albumin-SMN treatment

Muscle atrophy is a hallmark pathology of SMA.[41] For this reason, we examined myofiber area size and central nucleation from AAV9-albumin-SMN treated mice compared to *Smn*$^{2B/+}$ controls (Fig. 7a). Myofiber cross-sectional area was significantly reduced in untreated P19 *Smn*$^{2B/-}$ mice ($P < 0.001$), and this reduction in myofiber size is restored following AAV9-albumin-SMN treatment, but not to that of a health littermate ($P = 0.0014$) (Fig. 7b and c). We also examined centralised nucleation in muscle, a sign of continual repair and immature myofibers.[42,43] We did not see a

following AAV9-albumin-SMN treatment, **c**. Western blot of iron metabolism markers heme oxygenase, transferrin in P19 and P65 untreated and treated *Smn*$^{2B/-}$ and *Smn*$^{2B/+}$ mice, (untreated *Smn*$^{2B/-}$ N = 2, untreated *Smn*$^{2B/+}$ N = 2, treated *Smn*$^{2B/-}$ N = 2, *Smn*$^{2B/+}$ N = 2), **d.** Quantification of heme oxygenase *HO-1* RT-qPCR (untreated *Smn*$^{2B/-}$ N = 3, untreated *Smn*$^{2B/+}$ N = 3, treated *Smn*$^{2B/-}$ N = 3, *Smn*$^{2B/+}$ N = 3), **e.** Quantification of transferrin RT-qPCR (untreated *Smn*$^{2B/-}$ N = 3, untreated *Smn*$^{2B/+}$ N = 3, treated *Smn*$^{2B/-}$ N = 3, *Smn*$^{2B/+}$ N = 3), **f.** Western blot of autophagy marker P62 in P19 and P65 untreated and treated *Smn*$^{2B/-}$ and *Smn*$^{2B/+}$ mice, (untreated *Smn*$^{2B/-}$ N = 2, untreated *Smn*$^{2B/+}$ N = 2, treated *Smn*$^{2B/-}$ N = 2, *Smn*$^{2B/+}$ N = 2), **g.** Triglyceride levels in untreated P19 *Smn*$^{2B/-}$mice, P65 treated *Smn*$^{2B/-}$ and *Smn*$^{2B/+}$ mice, (untreated *Smn*$^{2B/-}$ N = 3, treated *Smn*$^{2B/-}$ N = 3, *Smn*$^{2B/+}$ N = 3), **h.** IGF1 protein levels in untreated P19 *Smn*$^{2B/+}$ and P65 treated *Smn*$^{2B/-}$ and *Smn*$^{2B/+}$ mice (untreated *Smn*$^{2B/-}$ N = 3, treated *Smn*$^{2B/-}$ N = 4, *Smn*$^{2B/+}$ N = 3) (T-test, **P ≤ 0.01, ***P ≤ 0.001, ****P ≤ 0.0001, ns = non-significant).

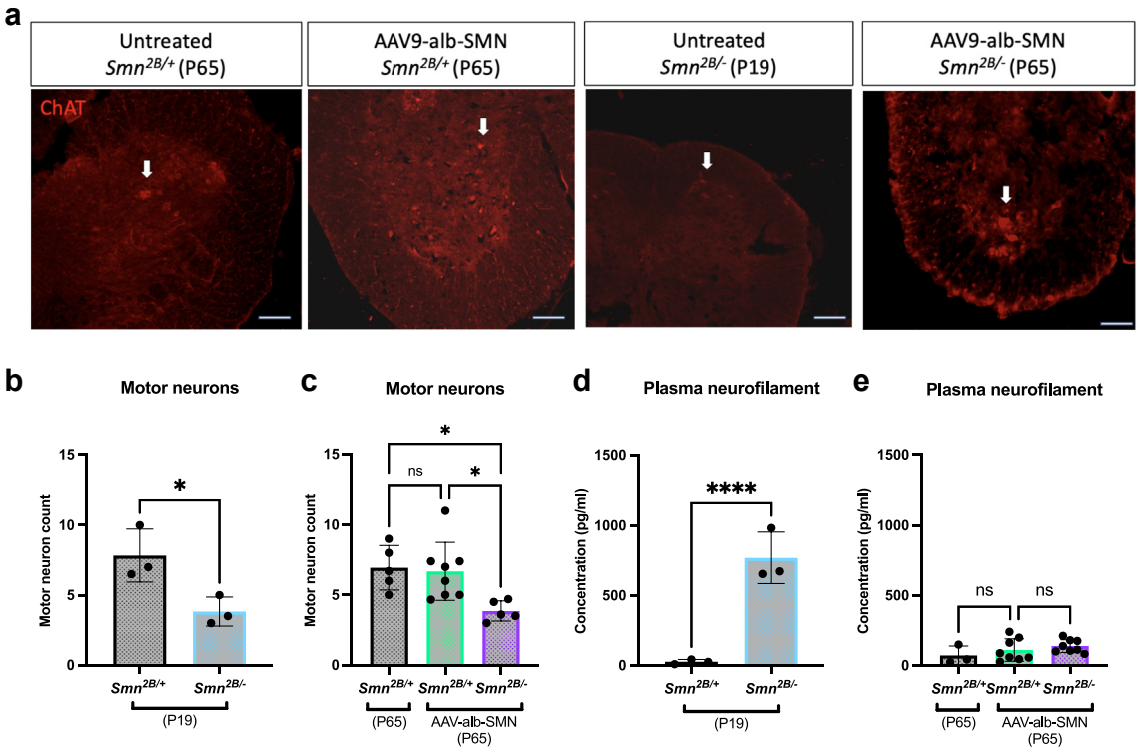

***Fig. 5:* Liver-SMN protein restoration partially rescues motor neuron pathology, a.** Representative ChAT-stained lumbar spinal cord sections from treated P65 $Smn^{2B/-}$ *mice,* treated P65 $Smn^{2B/+}$ mice, untreated P19 $Smn^{2B/-}$ mice and untreated P65 $Smn^{2B/+}$ mice (Scale bar 100 μm), **b.** Motor neuron cell body counts in untreated P19 $Smn^{2B/+}$ and $Smn^{2B/-}$mice ($Smn^{2B/-}$ N = 3, $Smn^{2B/+}$ N = 3), **c.** Motor neuron cell body counts in untreated P65 $Smn^{2B/+}$ and treated P65 $Smn^{2B/+}$ and $Smn^{2B/-}$mice (untreated $Smn^{2B/+}$ N = 5, treated $Smn^{2B/+}$ N = 8, $Smn^{2B/-}$ N = 5), **d.** Plasma neurofilament levels in untreated P19 $Smn^{2B/+}$ and $Smn^{2B/-}$mice ($Smn^{2B/-}$ N = 3, $Smn^{2B/+}$ N = 3), **e.** Plasma neurofilament levels in untreated P65 $Smn^{2B/+}$ and treated P65 $Smn^{2B/+}$ and $Smn^{2B/-}$mice (untreated $Smn^{2B/+}$ N = 3, treated $Smn^{2B/+}$ N = 8, $Smn^{2B/-}$ N = 8) (T-test, one-way ANOVA, *P ≤ 0.05, ****P ≤ 0.0001, ns = non-significant).

significant increase in untreated $Smn^{2B/-}$ mice, however this could be due to sample size (P > 0.05) (Fig. 7d). We saw a significant increase in the number of centralised nuclei in treated $Smn^{2B/-}$ mice compared to $Smn^{2B/+}$ mice (P = 0.0049) (Fig. 7e). While muscle growth seems to be restored as a product of liver-SMN protein restoration, we see here that an exclusive increase of SMN in the liver does not rescue muscle pathology in $Smn^{2B/-}$ mice, with muscle still in a state of immaturity or repair.

Pancreas cell fate imbalance is rescued following AAV9-albumin-SMN treatment in $Smn^{2B/-}$ mice

Finally, we investigated an additional peripheral pathology prevalent in $Smn^{2B/-}$ mice. The liver and pancreas are closely associated as the two organs that regulate blood sugar levels.[44] Untreated $Smn^{2B/-}$ mice present with pancreatic islet cell fate imbalance, obscuring hormonal release in response to blood sugar levels.[17] This ultimately affects liver glucose production leading to hyperglucagonemia and glucose resistance.[17] We confirmed an imbalance of pancreatic cell fate in untreated $Smn^{2B/-}$ mice (Fig. 8a and b). Specifically, untreated $Smn^{2B/-}$ mice display a decrease in insulin (β) producing cells at P19 (P = 0.0042) and demonstrate a rescue in the number of these cells following AAV9-albumin-SMN treatment (Fig. 8c). Similarly, we confirmed an increase in glucagon (α) producing cells in untreated P19 $Smn^{2B/-}$ mice (P = 0.0044) and found liver-specific SMN protein restoration was sufficient to normalise glucagon producing cell numbers to that of healthy controls (Fig. 8d and e). Treatment of AAV9-albumin-SMN in $Smn^{2B/-}$ mice restored balance to the essential pancreatic islet α/β cell ratio.

Discussion

While there is increasing evidence to suggest liver pathology is present in human SMA patients and mouse models, whether the liver phenotype is a direct result of intrinsic SMN protein depletion or a bystander of extrinsic SMN protein depletion is yet to be investigated.[15,22,25,45] In this study, we have demonstrated that the fatty liver phenotype in $Smn^{2B/-}$ mice is an

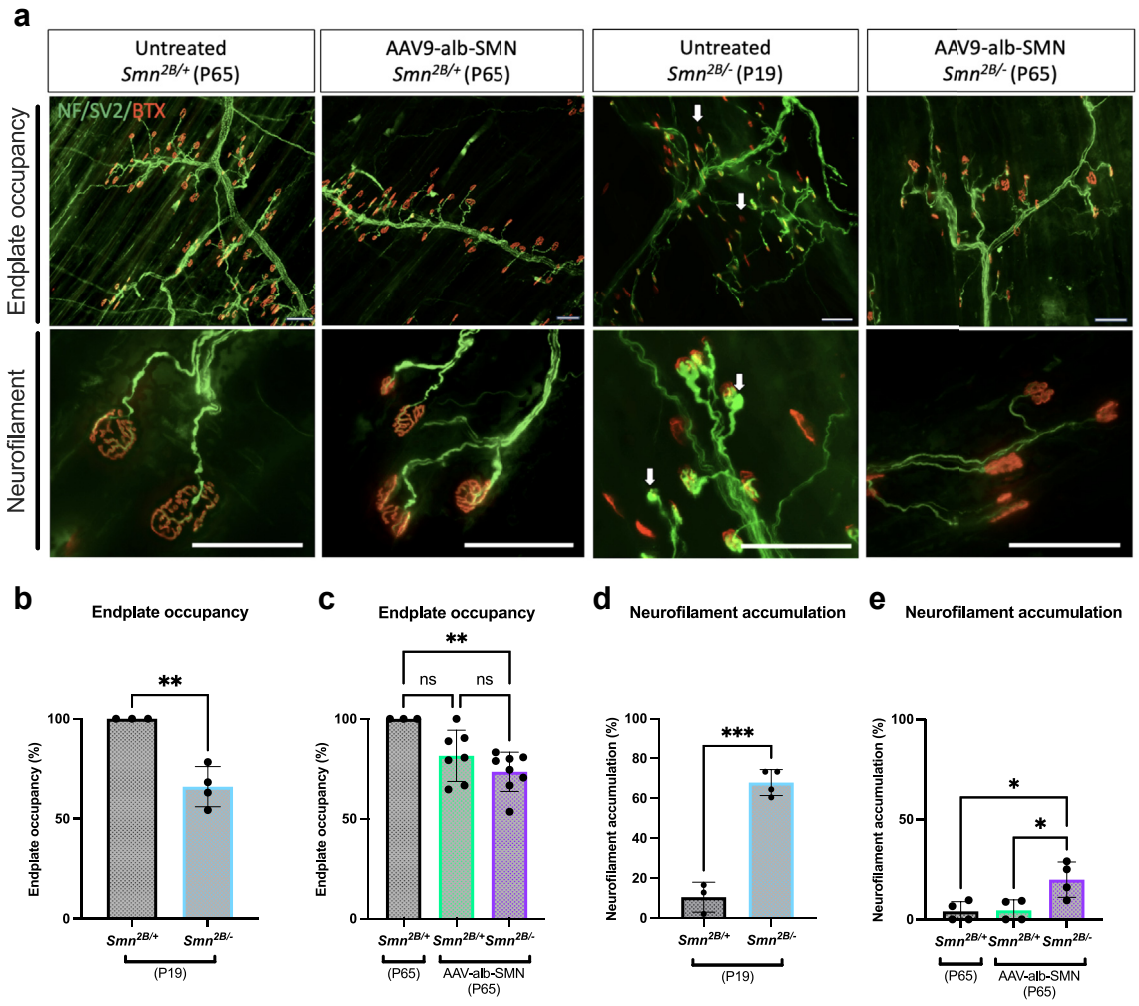

Fig. 6: **Liver-SMN protein restoration partially rescues neuromuscular junction pathology, a.** Representative neuromuscular junction images of occupied and unoccupied endplates (scale bar 50 μm) and neurofilament accumulation (scale bar 100 μm) from treated P65 *Smn*$^{2B/-}$ *mice,* treated P65 *Smn*$^{2B/+}$ mice, untreated P19 *Smn*$^{2B/-}$ mice and untreated P65 *Smn*$^{2B/+}$ mice, **b.** Endplate occupancy in untreated P19 *Smn*$^{2B/+}$ and *Smn*$^{2B/-}$mice (*Smn*$^{2B/-}$ N = 3, *Smn*$^{2B/+}$ N = 3), **c.** Endplate occupancy in untreated P65 *Smn*$^{2B/+}$ and treated P65 *Smn*$^{2B/+}$ and *Smn*$^{2B/-}$mice (untreated *Smn*$^{2B/+}$ N = 3, treated *Smn*$^{2B/+}$ N = 7, *Smn*$^{2B/-}$ N = 8), **d.** Neurofilament accumulation in untreated P19 *Smn*$^{2B/+}$ and *Smn*$^{2B/-}$mice (*Smn*$^{2B/-}$ N = 4, *Smn*$^{2B/+}$ N = 3), **e.** Neurofilament accumulation in untreated P65 *Smn*$^{2B/+}$ and treated P65 *Smn*$^{2B/+}$ and *Smn*$^{2B/-}$mice (untreated *Smn*$^{2B/+}$ N = 4, treated *Smn*$^{2B/+}$ N = 4, *Smn*$^{2B/-}$ N = 4) (T-test, one-way ANOVA, *P ≤ 0.05, ***P ≤ 0.001).

intrinsic impact of SMN protein depletion. AAV9-albumin-SMN treatment successfully resulted in a liver-specific increase of human SMN transcript and protein expression, with no detectable increase in the spinal cord or muscle, regardless of delivery route (ICV or IV). Notably, we saw no detectable expression of human SMN in livers of treated control mice (*Smn*$^{2B/+}$). As it is known SMN protein expression is high during early development and declines progressively with age, we speculate that a mechanism may be in place to ensure low levels of SMN during adulthood in *Smn*$^{2B/+}$ mice, and that these levels were likely below the level of detection possible by immunoblot.[46,47]

Although AAV9-albumin-SMN was designed to cause an increase in SMN protein levels in the liver, it is possible that a small amount of this protein is released by the liver and enters the circulation, subsequently distributing to CNS and peripheral tissues. Specifically, this could occur through extracellular vesicles (EVs), small membrane bound particles reported to carry proteins, lipids and nucleic acids throughout the body to mediate cell–cell communication.[48–53] For this reason we performed two specialised methods to detect both SMN mRNA and protein levels. Following AAV9-albumin-SMN treatment both mRNA transcripts (*SMN1*) and protein (SMN) levels in the brain, spinal cord and

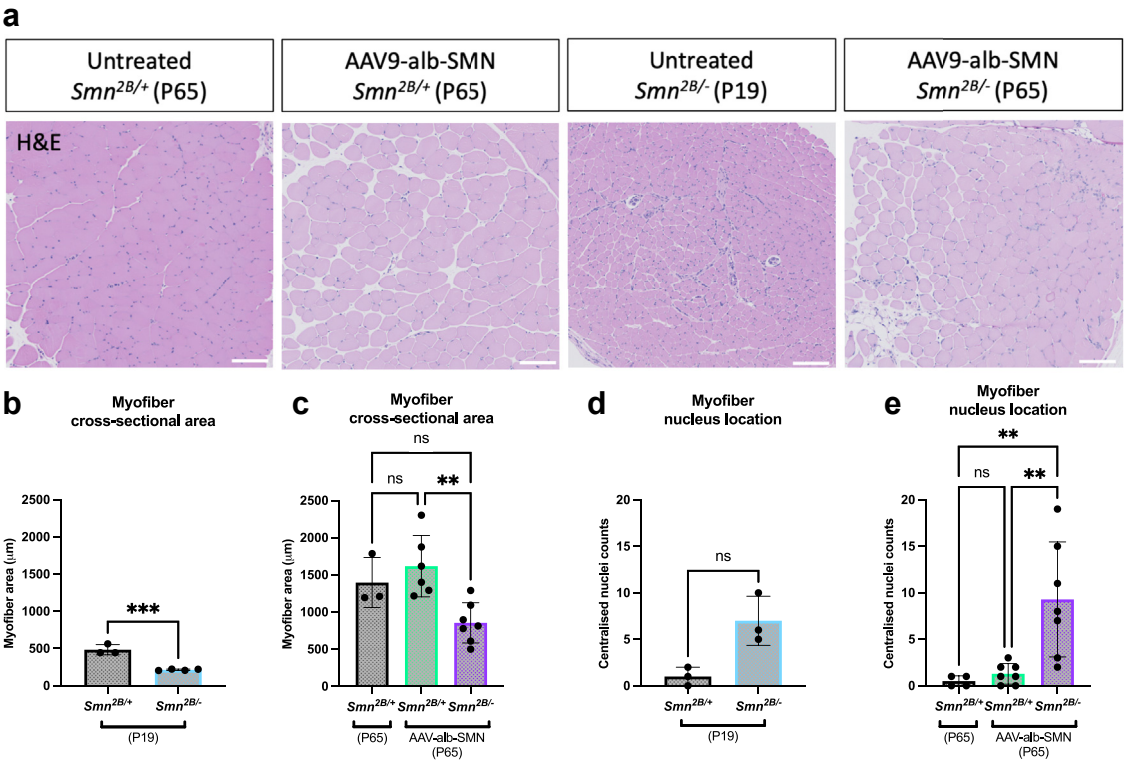

***Fig. 7*: Liver-SMN protein restoration rescues myofiber area but not centralised nucleation, a.** Representative myofiber cross-sectional area images from treated P65 *Smn*$^{2B/-}$ *mice,* treated P65 *Smn*$^{2B/+}$ mice, untreated P19 *Smn*$^{2B/-}$ mice and untreated P65 *Smn*$^{2B/+}$ mice (scale bar 50 µm), **b.** Myofiber area in untreated P19 *Smn*$^{2B/+}$ and *Smn*$^{2B/-}$mice (*Smn*$^{2B/-}$ N = 4, *Smn*$^{2B/+}$ N = 3), **c.** Myofiber area in untreated P65 *Smn*$^{2B/+}$ and treated P65 *Smn*$^{2B/+}$ and *Smn*$^{2B/-}$mice (untreated *Smn*$^{2B/+}$ N = 3, treated *Smn*$^{2B/+}$ N = 6, *Smn*$^{2B/-}$ N = 7), **d.** Nucleus location in untreated P19 *Smn*$^{2B/+}$ and *Smn*$^{2B/-}$mice (*Smn*$^{2B/-}$ N = 3, *Smn*$^{2B/+}$ N = 3), **e.** Nucleus location in untreated P65 *Smn*$^{2B/+}$ and treated P65 *Smn*$^{2B/+}$ and *Smn*$^{2B/-}$mice (untreated *Smn*$^{2B/+}$ N = 4, treated *Smn*$^{2B/+}$ N = 7, *Smn*$^{2B/-}$ N = 7) (T-test, one-way ANOVA, **P ≤ 0.01, ***P ≤ 0.001).

muscle are extremely low, and in some cases below the threshold of detection. We specifically demonstrate that *SMN1* mRNA expression in the CNS and muscles from AAV9-albumin-SMN treated *Smn*$^{2B/-}$ mice is significantly lower than expression levels seen in the spinal cord following AAV9-cba-SMN treatment. We can therefore presume, that such levels from circulating EVs would not make a meaningful impact on peripheral tissues and phenotypic outcomes of *Smn*$^{2B/-}$ mice after treatment with AAV9-albumin-SMN.

Following confirmation of SMN protein expression in the liver, we firstly examined whether this liver intrinsic restoration of SMN protein could rescue the fatty liver phenotype. Untreated *Smn*$^{2B/-}$ mice develop liver microvesicular steatosis within two weeks post birth and display iron metabolism defects as well as a reduction of plasma IGF-1 protein.[15] We observed a rescue in liver steatosis and lipid droplet accumulation in *Smn*$^{2B/-}$ AAV9-albumin-SMN treated mice. Specifically, liver steatosis was closely restored back to that of a healthy littermate (*Smn*$^{2B/+}$). Aspects of liver function were also restored in treated *Smn*$^{2B/-}$ mice, levels of iron metabolism enzyme heme oxygenase (HO-1) were like that of the control *Smn*$^{2B/+}$ mice. HO-1 degrades heme to iron, carbon monoxide and biliverdin. Upon liver insult HO-1 is overexpressed by means of a protective mechanism to prevent damage, in line with an increase of HO-1 in untreated *Smn*$^{2B/-}$ mice.[15,54] As such the reduction in HO-1 following AAV9-albumin-SMN treatment would suggest in part, restoration of iron metabolism.

Plasma IGF-1 protein levels were also rescued in *Smn*$^{2B/-}$ treated mice. As liver IGF-1 regulates insulin sensitivity, inflammation, oxidative stress, and mitochondrial function, it's restoration should lead to enhanced pancreatic β-cell function. Therefore, increased IGF-1 following liver intrinsic SMN protein augmentation is likely to contribute to the rescue of insulin and glucagon cell fate imbalance seen in the pancreas of untreated *Smn*$^{2B/-}$ mice.[17] Additionally, we found triglyceride levels were restored in *Smn*$^{2B/-}$ treated mice to that of healthy littermates (*Smn*$^{2B/+}$). High levels of triglycerides in the blood and increased storage of fat in the liver is a distinctive feature of fatty

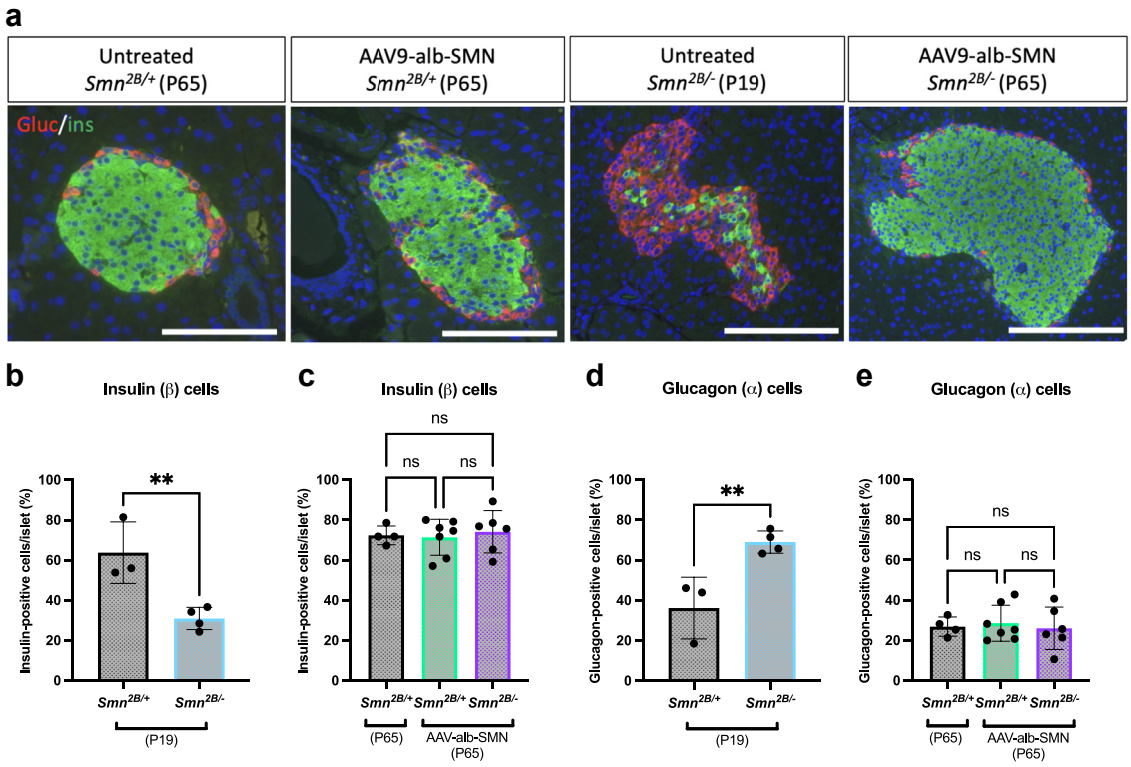

Fig. 8: **Pancreatic islets cell fate imbalance is rescued following treatment with AAV9-albumin-SMN, a.** Representative images of pancreatic islets from treated P65 *Smn*$^{2B/-}$ *mice,* treated P65 *Smn*$^{2B/+}$ mice, untreated P19 *Smn*$^{2B/-}$ mice and untreated P65 *Smn*$^{2B/+}$ mice (scale bar 100 μm), staining glucagon and insulin (Gluc/ins) producing cells, **b.** Insulin-producing alpha-cells in untreated P19 *Smn*$^{2B/+}$ and *Smn*$^{2B/-}$ mice (*Smn*$^{2B/-}$ N = 4, *Smn*$^{2B/+}$ N = 3), **c.** Insulin-producing alpha-cells in untreated P65 *Smn*$^{2B/+}$ and treated P65 *Smn*$^{2B/+}$ and *Smn*$^{2B/-}$ mice (untreated *Smn*$^{2B/+}$ N = 4, treated *Smn*$^{2B/+}$ N = 7, *Smn*$^{2B/-}$ N = 6), **d.** Glucagon-producing beta-cells in untreated P19 *Smn*$^{2B/+}$ and *Smn*$^{2B/-}$ mice (*Smn*$^{2B/-}$ N = 4, *Smn*$^{2B/+}$ N = 3), **e.** Glucagon-producing beta-cells in untreated P65 *Smn*$^{2B/+}$ and treated P65 *Smn*$^{2B/+}$ and *Smn*$^{2B/-}$ mice, (untreated *Smn*$^{2B/+}$ N = 4, treated *Smn*$^{2B/+}$ N = 7, *Smn*$^{2B/-}$ N = 6) (T-test, one-way ANOVA, **P ≤ 0.01, ns = non-significant).

liver disease (MASLD), and prevention of hepatic accumulation of triglycerides is indicative of improved liver function.

Secondly, we investigated whether the fatty liver rescue due to liver specific transgene expression had a broader impact on central and peripheral tissues. A distinguished pathology in SMA is the rapid neurodegeneration of lower motor neurons that occurs around the time of disease onset with evidence of presymptomatic loss in some patients with SMA.[55,56] For this reason, we examined motor neuron cell body loss, indicative of neurodegeneration. SMN protein restoration in the liver was not enough to rescue motor neuron loss in *Smn*$^{2B/-}$ mice. This is likely representative of slow axonal degeneration over time ultimately leading to irreversible cell death.[57] The inability to reverse motor neuron cell body loss supports the notion that motor neuron loss is at least in part a cell autonomous effect of SMN protein insufficiency and that SMA may be a developmental disease.[10] Similarly, rescue of liver pathology via ICV or IV administration did not reduce pathological levels of neurofilament in plasma at P19. However, treatment was sufficient to reduce pathological neurofilament levels at P65. This may be reflective of a developmental change, NMJ health or liver-mediated neuroprotection in other regions such as the peripheral nervous system (PNS).[58,59] Liver SMN protein expression, therefore, does impact neurofilament levels after early neuronal loss and alludes to the importance of postnatal peripheral SMN protein expression. Ultimately, post-symptomatic depletion of SMN protein in the motor neuron may not be as detrimental as ubiquitously depleting the protein across the entire body.[10]

We also examined two specific defects at the level of the NMJ; endplate occupancy, reduced in untreated *Smn*$^{2B/-}$ mice, and neurofilament accumulation, increased in untreated *Smn*$^{2B/-}$ mice.[60] We show that AAV9-albumin-SMN treatment was insufficient to fully restore endplate occupancy in *Smn*$^{2B/-}$ mice, therefore liver SMN protein expression is not sufficient to prevent CNS pathology. Furthermore, loss of SMN protein before NMJ maturation results in a severe SMA

phenotype whereby antisense-oligonucleotide (ASO) SMN restoration, administered at P1, was not adequate to produce complete NMJ recovery.[61] Therefore, postnatal delivery of SMN protein, at the liver or elsewhere, may not be enough to fully restore the neuromuscular unit. Taken together the lack of impact liver-SMN protein expression has on central pathologies could be explained by a developmental aspect of SMA, requiring early, pre-natal SMN restoration for optimal therapeutic outcome.[62–64]

Alternatively, we demonstrate reduced neurofilament accumulation at the NMJ in *Smn*$^{2B/-}$ treated mice. Previous findings report neurofilament accumulation is present before the onset of denervation suggesting the two pathologies may not be stringently correlated.[65] We confirm neurofilament engulfs endplates in untreated *Smn*$^{2B/-}$ mice while a significant reduction in this accumulation is seen in AAV9-albumin-SMN treated *Smn*$^{2B/-}$ mice, likely improving the transport of components needed for maturation and maintenance of the NMJ.[66] For the remaining occupied NMJs, this reduction in neurofilament accumulation will have enabled vital cellular transport and regulation of axonal transport machinery which could have contributed to the increased survival of treated *Smn*$^{2B/-}$ mice.[67] To an extent, this would help stabilise the neuromuscular unit. However, without innervation motor nerve terminal neurotransmission is lost, consequently preventing muscle contraction.[68]

As we saw a rescue of muscle fibre cross-sectional area but not NMJ occupancy, we demonstrate an impact of liver-SMN protein on intrinsic muscle health; perhaps enough to rescue growth but not complete functionality. Our treated mice had significantly improved neuromuscular coordination, but this was not a comprehensive rescue as hind limb deterioration and scoliosis were visible later in the disease (P150^{+}). It is important to note that untreated *Smn*$^{2B/-}$ mice are unable to perform the rotarod test due to severe muscle weakness and balance, for this reason we speculate that if comparison was possible between untreated *Smn*$^{2B/-}$ mice and treated *Smn*$^{2B/-}$ mice that a significant improvement in rotarod time in the treated group would have been found. Importantly, we also display a significant improvement in the ability of *Smn*$^{-/-}$*;SMN2;Δ7* mice to right themselves following treatment. The pathophysiology of AAV9-albumin-treated *Smn*$^{2B/-}$ mice would suggest a delayed deterioration in neuromuscular coordination. Additionally, we found the majority of myofibers had mispositioned myonuclei, indicative of immaturity and continual myofiber repair.[43] While we demonstrate a significant improvement in neuromuscular ability following AAV9-albumin-SMN treatment, ultimately, the muscle was not fully functional.

Importantly, we show rescuing intrinsic SMN levels in the liver has wide-reaching effects on additional central and peripheral defects. The reasons behind the impact of liver SMN protein on a multitude of SMA pathologies is yet to be discovered. The liver is a vital endocrine organ that has been implicated in several CNS (liver-brain) and peripheral-axis (liver-pancreas-gut).[44,69] We speculate an extra-neuronal role of neurotrophic factors could be involved.[70–72] Recent evidence demonstrates several neurotrophic factors and their receptors are expressed in hepatic cells and are involved in insulin regulation, lipid homeostasis and liver cell injury and fibrosis.[73,74] In particular, IGF-1 is a potent neurotrophic factor, mainly secreted by the liver, that plays a crucial role in the PNS and CNS. Depleted IGF-1 levels reported in *Smn*$^{2B/-}$ mice were restored following AAV9-albumin-SMN treatment.[15] Importantly, growth hormone (GH), secreted by the pituitary gland leads to the secretion of IGF-1, mainly by the liver.[75] Previous work has demonstrated protective effects of MR-409 treatment, an agonist of GH, attenuated muscle atrophy and delayed alpha motor neuron death in SMNΔ7 mice.[76] IGF-1 is known to modulate the PI3K/Akt pathway improving muscle atrophy and neurite outgrowth.[75,77] The GH/IGF-1 axis could therefore play a pivotal role in the ability of liver-SMN to impact whole-body pathologies in SMA.[76,78]

Furthermore, the liver–muscle axis warrants further investigation in the context of SMA pathology, not only does MASLD severity correlate with sarcopenia, the loss of muscle mass and muscle strength, but hepatic steatosis also contributes to muscle insulin-resistance via influence on muscle protein metabolism.[79] As we are aware, *Smn*$^{2B/-}$ mice show hepatic insulin resistance, and an increase in insulin resistance has been shown to mediate decreased glucose uptake in skeletal muscle as well as decreased hepatic glucose usage.[15,80] Ultimately, this can lead to elevated levels of plasma glucose and triglycerides, eventually accumulating in the liver.[80] Therefore, pancreatic cell fate imbalance seen in *Smn*$^{2B/-}$ mice, restored by liver directed SMN protein expression, is likely a compensatory mechanism in an attempt to restore energy homeostasis.[17] Investigation into this inter-organ cross talk between the liver and the muscle has identified the liver secretome as a possible contributor to the development of muscle atrophy, via an increase in catabolic effectors such as hepatokines.[79,81] SMA patients may have an increased risk for an altered liver metabolome which could explain liver involvement in disease pathophysiology.[24]

The amelioration of liver pathology as well as several CNS and peripheral pathologies, likely explains the increase in weight, neuromuscular coordination and survival in treated cohorts beyond that of untreated *Smn*$^{2B/-}$ mice. The survival of AAV9-albumin-SMN treated *Smn*$^{2B/-}$ mice (median survival 205 days) was increased by 9.7% compared to untreated *Smn*$^{2B/-}$ mice (median survival 20 days) and was 23% that of a healthy littermate (*Smn*$^{2B/+}$). It is unclear whether the difference in lifespan between treated *Smn*$^{2B/-}$ mice and controls

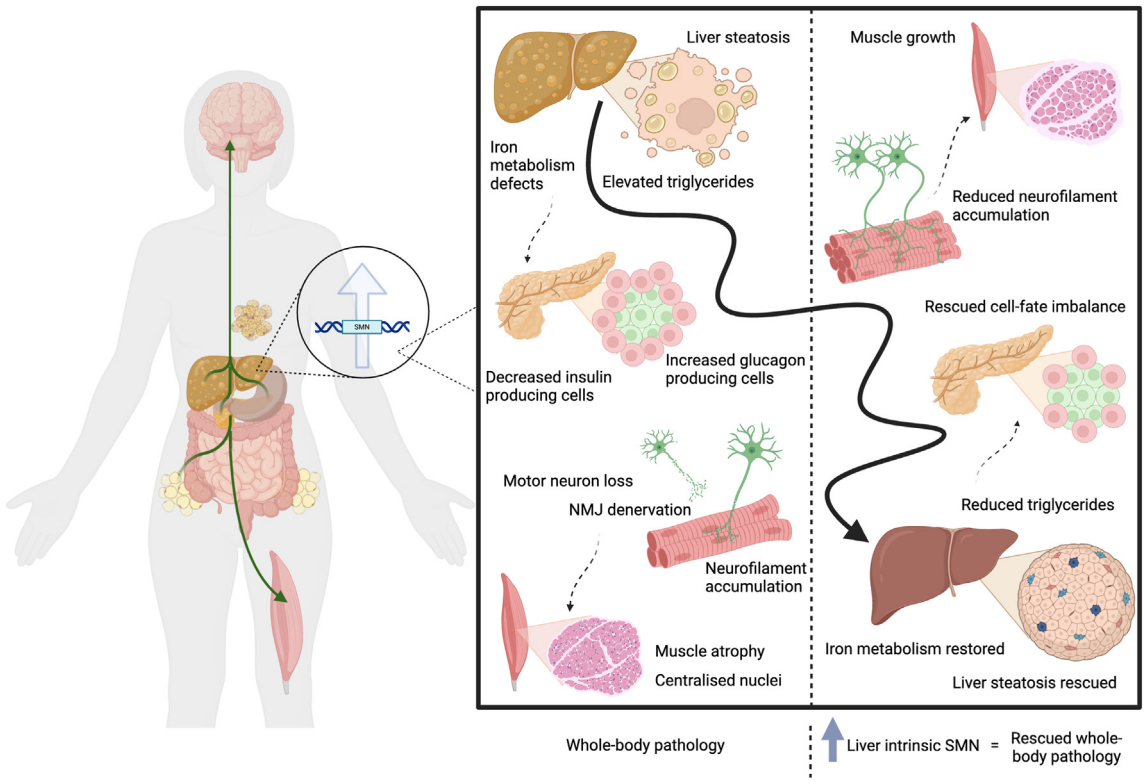

***Fig. 9:* Schematic summarising the effect of liver intrinsic SMN on whole-body pathologies in SMA,** Whole-body pathologies present in untreated *Smn*$^{2B/-}$ mice (liver steatosis, pancreatic cell fate imbalance, motor neuron loss, NMJ denervation and muscle atrophy). Pathologies rescued following AAV9-albumin-SMN treatment (reduced liver steatosis, pancreatic cell fate balance, reduced neurofilament accumulation and increased myofiber area).

(*Smn*$^{2B/+}$) was due to loss of transgene expression in hepatocytes, and the livers regenerative capacity, or whether liver-exclusive SMN increase is not enough to fully rescue survival as is seen with whole-body SMN correction.[82,83] Furthermore, while the albumin promoter is widely used for liver-specific transgene expression, off–target activity cannot be ruled out, leading to unintended gene expression in non-hepatic tissues. This leakage, or reduced specificity could impact therapeutic outcomes where precise gene regulation is required. In this study we made every effort to confirm the specificity of gene expression to the liver using both RT-qPCR and immunoblot, ensuring that any non-specific expression was detected, if present, outside the liver. Additionally, AAV genomes typically remain episomal meaning *SMN1* expression will dilute out of hepatocytes overtime, and use of AAV could therefore become a limiting factor if trying to assess the long-term impact of *SMN1* correction in the liver. Another limiting factor could be the use of the less severe mouse model of SMA. While the *Smn*$^{2B/-}$ model was meticulously selected for this study due to the presence of peripheral pathologies, a more in-depth analysis should be conducted on the more severe model of SMA e.g. SMNΔ7 mice.

Overall, our results suggest liver-SMN protein depletion is likely contributing to central and peripheral pathologies in SMA and highlights the importance of understanding peripheral defects to maximise clinical outcomes. A systemic approach to therapy targeting both peripheral and CNS defects during early development is likely key to finding a cure for SMA.[4,84,85] The impact, shown in this study, of liver SMN protein restoration on whole-body pathology demonstrates the importance of liver intrinsic SMN protein and suggests the liver could be having a broader impact on pathology than previously thought.

Conclusion

Here, we are implementing liver SMN protein depletion as a contributor to SMA whole-body pathophysiology (Fig. 9). By using an AAV9 delivering *SMN1* driven by a liver-specific promoter, we successfully generated a liver-targeted SMN protein-rescue mouse model. This enabled us to study whether liver pathology was an

intrinsic or extrinsic impact of SMN protein depletion. We found rescue of SMN protein in the liver alone was enough to improve various CNS and peripheral pathologies known to SMA (Fig. 9). This work provides insight into the contribution of liver pathology in SMA and will improve our understanding of SMA as a multisystem disorder.

Contributors

E.R.S, M.O.D and R.K designed the research, E.R.S, A.B, R.Y, A.R, K.P, M.M.A.A. and Y.D.R performed the experiments, B.L.S, R.P, K.P provided material support, E.R.S, A.B. and R.Y. analysed and verified the data, E.R.S.—writing—original draft, R.K., M.O.D, E.R.S—writing—review & editing. All authors have read and approved the final version of the manuscript.

Data sharing statement

All data associated with this study are available in the main text or supplementary materials. Raw data can be provided upon request.

Declaration of interests

R.K. is a member of the scientific advisory board for Cure SMA. The authors disclose no conflicts of interest.

Acknowledgements

The authors thank the University of Ottawa Animal Behaviour and Physiology core for providing motor function test equipment. We are grateful to the Kothary laboratory for research related discussions. We would like to thank Charlotte René for providing the human fibroblast cell line and for her critical reading of the manuscript. This work was supported by Muscular Dystrophy Association (USA) [grant number 963652 to R.K.]; the Canadian Institutes of Health Research [grant number PJT-186300 to R.K.]; the Fredrick Banting and Charles Best Canadian Institutes of Health Research Doctoral Research Award to A.R.; the University of Ottawa Brain and Mind Institute CNMD STAR Award to E.S.; and the uOBMRI Trainee Researchers in Multiple Sclerosis Award to M.M.A.A.

Appendix A. Supplementary data

Supplementary data related to this article can be found at https://doi.org/10.1016/j.ebiom.2024.105444.

References

1 Lefebvre S, Bürglen L, Reboullet S, et al. Identification and characterization of a spinal muscular atrophy-determining gene. *Cell*. 1995;80:155–165.
2 Burnett BG, Muñoz E, Tandon A, Kwon DY, Sumner CJ, Fischbeck KH. Regulation of SMN protein stability. *Mol Cell Biol*. 2009;29:1107–1115.
3 Lefebvre S, Burlet P, Liu Q, et al. Correlation between severity and SMN protein level in spinal muscular atrophy. *Nat Genet*. 1997;16:265–269.
4 Chaytow H, Faller KME, Huang YT, Gillingwater TH. Spinal muscular atrophy: from approved therapies to future therapeutic targets for personalized medicine. *Cell Rep Med*. 2021;21(2):100346.
5 Poirier A, Weetall M, Heinig K, et al. Risdiplam distributes and increases SMN protein in both the central nervous system and peripheral organs. *Pharmacol Res Perspect*. 2018;6:e00447.
6 Thomsen G, Burghes AHM, Hsieh C, et al. Biodistribution of onasemnogene abeparvovec DNA, mRNA and SMN protein in human tissue. *Nat Med*. 2021;27:1701–1711.
7 Finkel RS, Chiriboga CA, Vajsar J, et al. Treatment of infantile-onset spinal muscular atrophy with nusinersen: a phase 2, open-label, dose-escalation study. *Lancet Lond Engl*. 2016;388:3017–3026.
8 Hamilton G, Gillingwater TH. Spinal muscular atrophy: going beyond the motor neuron. *Trends Mol Med*. 2013;19:40–50.
9 Novelli G, Calzà L, Amicucci P, et al. Expression study of survival motor neuron gene in human fetal tissues. *Biochem Mol Med*. 1997;61:102–106.
10 Park GH, Maeno-Hikichi Y, Awano T, Landmesser LT, Monani UR. Reduced survival of motor neuron (SMN) protein in motor neuronal progenitors functions cell autonomously to cause spinal muscular atrophy in model mice expressing the human centromeric (SMN2) gene. *J Neurosci*. 2010;30:12005–12019.
11 Castillo-Armengol J, Fajas L, Lopez-Mejia IC. Inter-organ communication: a gatekeeper for metabolic health. *EMBO Rep*. 2019;20:e47903.
12 Watt MJ, Miotto PM, De Nardo W, Montgomery MK. The liver as an endocrine organ-linking NAFLD and insulin resistance. *Endocr Rev*. 2019;40:1367–1393.
13 Szunyogova E, Zhou H, Maxwell GK, et al. Survival Motor Neuron (SMN) protein is required for normal mouse liver development. *Sci Rep*. 2016;6:34635.
14 Vitte JM, Davoult B, Roblot N, et al. Deletion of murine smn exon 7 directed to liver leads to severe defect of liver development associated with iron overload. *Am J Pathol*. 2004;165:1731–1741.
15 Deguise MO, Pileggi C, De Repentigny Y, et al. SMN depleted mice offer a robust and rapid onset model of nonalcoholic fatty liver disease. *Cell Mol Gastroenterol Hepatol*. 2021;12:354–377.e3.
16 Bowerman M, Murray LM, Beauvais A, Pinheiro B, Kothary R. A critical smn threshold in mice dictates onset of an intermediate spinal muscular atrophy phenotype associated with a distinct neuromuscular junction pathology. *Neuromuscul Disord*. 2012;22:263–276.
17 Bowerman M, Swoboda KJ, Michalski JP, et al. Glucose metabolism and pancreatic defects in spinal muscular atrophy. *Ann Neurol*. 2012;72:256–268.
18 Hua Y, Sahashi K, Rigo F, et al. Peripheral SMN restoration is essential for long-term rescue of a severe spinal muscular atrophy mouse model. *Nature*. 2011;478:123–126.
19 Reilly A, Deguise MO, Beauvais A, et al. Central and peripheral delivered AAV9-SMN are both efficient but target different pathomechanisms in a mouse model of spinal muscular atrophy. *Gene Ther*. 2022;29:544–554.
20 Riessland M, Ackermann B, Förster A, et al. SAHA ameliorates the SMA phenotype in two mouse models for spinal muscular atrophy. *Hum Mol Genet*. 2010;19:1492–1506.
21 Crawford TO, Sladky JT, Hurko O, Besner-Johnston A, Kelley RI. Abnormal fatty acid metabolism in childhood spinal muscular atrophy. *Ann Neurol*. 1999;45:337–343.
22 Deguise MO, Baranello G, Mastella C, et al. Abnormal fatty acid metabolism is a core component of spinal muscular atrophy. *Ann Clin Transl Neurol*. 2019;6:1519–1532.
23 Yeo CJJ, Levine A, Darras B. Hepatic steatosis in patients with spinal muscular atrophy (SMA) (P1-1.Virtual). *Neurology*. 2022;98(18):2692.
24 Naume MM, Jørgensen MH, Høi-Hansen CE, et al. Metabolic assessment in children with neuromuscular disorders shows risk of liver enlargement, steatosis and fibrosis. *Acta Paediatr*. 2023;112:846–853.
25 Yeo CJJ, Darras BT. Overturning the paradigm of spinal muscular atrophy as Just a motor neuron disease. *Pediatr Neurol*. 2020;109:12–19.
26 Eshraghi M, McFall E, Gibeault S, Kothary R. Effect of genetic background on the phenotype of the Smn2B/- mouse model of spinal muscular atrophy. *Hum Mol Genet*. 2016;25:4494–4506.
27 Blessing D, Vachey G, Pythoud C, et al. Scalable production of AAV vectors in orbitally shaken HEK293 cells. *Mol Ther Methods Clin Dev*. 2019;13:14–26.
28 Gorski K, Carneiro M, Schibler U. Tissue-specific in vitro transcription from the mouse albumin promoter. *Cell*. 1986;47:767–776.
29 Shafey D, Boyer JG, Bhanot K, Kothary R. Identification of novel interacting protein partners of SMN using tandem affinity purification. *J Proteome Res*. 2010;9:1659–1669.
30 Deguise MO, De Repentigny Y, Tierney A, et al. Motor transmission defects with sex differences in a new mouse model of mild spinal muscular atrophy. *EBioMedicine*. 2020;55:102750.
31 Murray L, Gillingwater TH, Kothary R. Dissection of the transversus abdominis muscle for whole-mount neuromuscular junction analysis. *J Vis Exp*. 2014;83:e51162.
32 Ripolone M, Ronchi D, Violano R, et al. Impaired muscle mitochondrial biogenesis and myogenesis in spinal muscular atrophy. *JAMA Neurol*. 2015;72:666–675.
33 Jin Q, Qiao C, Li J, Li J, Xiao X. An engineered serum albumin-binding AAV9 capsid achieves improved liver transduction after intravenous delivery in mice. *Gene Ther*. 2020;27:237–244.
34 Sands MS. AAV-mediated liver-directed gene therapy. *Methods Mol Biol Clifton NJ*. 2011;807:141–157.

35 Groen EJN, Perenthaler E, Courtney NL, et al. Temporal and tissue-specific variability of SMN protein levels in mouse models of spinal muscular atrophy. *Hum Mol Genet*. 2018;27:2851–2862.
36 Cunningham SC, Dane AP, Spinoulas A, Logan GJ, Alexander IE. Gene delivery to the juvenile mouse liver using AAV2/8 vectors. *Mol Ther J Am Soc Gene Ther*. 2008;16:1081–1088.
37 Lavrovsky Y, Song CS, Chatterjee B, Roy AK. Age-dependent increase of heme oxygenase–1 gene expression in the liver mediated by NFκB. *Mech Ageing Dev*. 2000;114:49–60.
38 Bloomer SA, Zhang HJ, Brown KE, Kregel KC. Differential regulation of hepatic heme oxygenase-1 protein with aging and heat stress. *J Gerontol Ser A*. 2009;64:419–425.
39 Monani UR. Spinal muscular atrophy: a deficiency in a ubiquitous protein; a motor neuron-specific disease. *Neuron*. 2005;48:885–896.
40 Murray LM, Beauvais A, Bhanot K, Kothary R. Defects in neuromuscular junction remodelling in the Smn(2B/-) mouse model of spinal muscular atrophy. *Neurobiol Dis*. 2013;49:57–67.
41 Kolb SJ, Kissel JT. Spinal muscular atrophy. *Neurol Clin*. 2015;33:831–846.
42 Folker ES, Baylies MK. Nuclear positioning in muscle development and disease. *Front Physiol*. 2013;4:363.
43 Yin H, Price F, Rudnicki MA. Satellite cells and the muscle stem cell niche. *Physiol Rev*. 2013;93:23–67.
44 Svegliati-Baroni G, Patrício B, Lioci G, Macedo MP, Gastaldelli A. Gut-pancreas-liver Axis as a target for treatment of NAFLD/NASH. *Int J Mol Sci*. 2020;21:5820.
45 Yeo CJJ, Levine A, Darras B. Hepatic steatosis in patients with spinal muscular atrophy (SMA) (P1-1.Virtual). *Neurology*. 2022;98(18 Supplement) [cited 2022 Jul 17]. Available from: https://n.neurology.org/content/98/18_Supplement/2692.
46 Jablonka S, Sendtner M. Developmental regulation of SMN expression: pathophysiological implications and perspectives for therapy development in spinal muscular atrophy. *Gene Ther*. 2017;24:506–513.
47 Ramos DM, d'Ydewalle C, Gabbeta V, et al. Age-dependent SMN expression in disease-relevant tissue and implications for SMA treatment. *J Clin Invest*. 2019;129:4817–4831.
48 Carpintero-Fernández P, Fafián-Labora J, O'Loghlen A. Technical advances to study extracellular vesicles. *Front Mol Biosci*. 2017;4:79.
49 Mulcahy LA, Pink RC, Carter DRF. Routes and mechanisms of extracellular vesicle uptake. *J Extracell Vesicles*. 2014;3.
50 René CA, Parks RJ. Delivery of therapeutic agents to the central nervous system and the promise of extracellular vesicles. *Pharmaceutics*. 2021;13:492.
51 Newman LA, Useckaite Z, Johnson J, Sorich MJ, Hopkins AM, Rowland A. Selective isolation of liver-derived extracellular vesicles redefines performance of miRNA biomarkers for non-alcoholic fatty liver disease. *Biomedicines*. 2022;10:195.
52 Royo F, Moreno L, Mleczko J, et al. Hepatocyte-secreted extracellular vesicles modify blood metabolome and endothelial function by an arginase-dependent mechanism. *Sci Rep*. 2017;7:42798.
53 Nash LA, McFall ER, Perozzo AM, et al. Survival motor neuron protein is released from cells in exosomes: a potential biomarker for spinal muscular atrophy. *Sci Rep*. 2017;7:13859.
54 Canesin G, Feldbrügge L, Wei G, et al. Heme oxygenase-1 mitigates liver injury and fibrosis via modulation of LNX1/Notch 1 pathway in myeloid cells. *iScience*. 2022;25:104983.
55 Finkel RS. Electrophysiological and motor function scale association in a pre-symptomatic infant with spinal muscular atrophy type I. *Neuromuscul Disord*. 2013;23:112–115.
56 Murray LM, Lee S, Bäumer D, Parson SH, Talbot K, Gillingwater TH. Pre-symptomatic development of lower motor neuron connectivity in a mouse model of severe spinal muscular atrophy. *Hum Mol Genet*. 2010;19:420–433.
57 Kong L, Valdivia DO, Simon CM, et al. Impaired prenatal motor axon development necessitates early therapeutic intervention in severe SMA. *Sci Transl Med*. 2021;13:eabb6871.
58 Dai Y, Dong J, Wu Y, et al. Enhancement of the liver's neuroprotective role ameliorates traumatic brain injury pathology. *Proc Natl Acad Sci U S A*. 2023;120:e2301360120.
59 Gonzalo-Gobernado R, Reimers D, Casarejos MJ, et al. Liver growth factor induces glia-associated neuroprotection in an in vitro model of Parkinson's disease. *Brain Sci*. 2020;10:315.
60 Murray LM, Comley LH, Thomson D, Parkinson N, Talbot K, Gillingwater TH. Selective vulnerability of motor neurons and dissociation of pre- and post-synaptic pathology at the neuromuscular junction in mouse models of spinal muscular atrophy. *Hum Mol Genet*. 2008;17:949–962.
61 Comley LH, Kline RA, Thomson AK, et al. Motor unit recovery following Smn restoration in mouse models of spinal muscular atrophy. *Hum Mol Genet*. 2022;31:3107–3119.
62 Rashnonejad A, Amini Chermahini G, Gündüz C, et al. Fetal gene therapy using a single injection of recombinant AAV9 rescued SMA phenotype in mice. *Mol Ther J Am Soc Gene Ther*. 2019;27:2123–2133.
63 Schwab ME, Shao S, Zhang L, et al. Investigating attitudes toward prenatal diagnosis and fetal therapy for spinal muscular atrophy. *Prenat Diagn*. 2022;42:1409–1419.
64 Tizzano EF, Zafeiriou D. Prenatal aspects in spinal muscular atrophy: from early detection to early presymptomatic intervention. *Eur J Paediatr Neurol*. 2018;22:944–950.
65 Kariya S, Park GH, Maeno-Hikichi Y, et al. Reduced SMN protein impairs maturation of the neuromuscular junctions in mouse models of spinal muscular atrophy. *Hum Mol Genet*. 2008;17:2552–2569.
66 Torres-Benito L, Ruiz R, Tabares L. Synaptic defects in spinal muscular atrophy animal models. *Dev Neurobiol*. 2012;72:126–133.
67 Kreutzer M, Seehusen F, Kreutzer R, et al. Axonopathy is associated with complex axonal transport defects in a model of multiple sclerosis. *Brain Pathol Zurich Switz*. 2012;22:454–471.
68 Boido M, Vercelli A. Neuromuscular junctions as key contributors and therapeutic targets in spinal muscular atrophy. *Front Neuroanat*. 2016;10:6.
69 Matsubara Y, Kiyohara H, Teratani T, Mikami Y, Kanai T. Organ and brain crosstalk: the liver-brain axis in gastrointestinal, liver, and pancreatic diseases. *Neuropharmacology*. 2022;205:108915.
70 Cassiman D, Denef C, Desmet VJ, Roskams T. Human and rat hepatic stellate cells express neurotrophins and neurotrophin receptors. *Hepatology*. 2001;33:148–158.
71 Mwangi SM, Peng S, Nezami BG, et al. Glial cell line-derived neurotrophic factor protects against high-fat diet-induced hepatic steatosis by suppressing hepatic PPAR-γ expression. *Am J Physiol Gastrointest Liver Physiol*. 2016;310:G103–G116.
72 Tao L, Ma W, Wu L, et al. Glial cell line-derived neurotrophic factor (GDNF) mediates hepatic stellate cell activation via ALK5/Smad signalling. *Gut*. 2019;68:2214–2227.
73 Kendall TJ, Hennedige S, Aucott RL, et al. p75 Neurotrophin receptor signaling regulates hepatic myofibroblast proliferation and apoptosis in recovery from rodent liver fibrosis. *Hepatology*. 2009;49:901–910.
74 Nakagawa T, Tsuchida A, Itakura Y, et al. Brain-derived neurotrophic factor regulates glucose metabolism by modulating energy balance in diabetic mice. *Diabetes*. 2000;49:436–444.
75 Ahmad SS, Ahmad K, Lee EJ, Lee YH, Choi I. Implications of insulin-like growth factor-1 in skeletal muscle and various diseases. *Cells*. 2020;9:1773.
76 Boido M, Gesmundo I, Caretto A, et al. Agonist of growth hormone-releasing hormone improves the disease features of spinal muscular atrophy mice. *Proc Natl Acad Sci U S A*. 2023;120:e2216814120.
77 Feldman EL, Sullivan KA, Kim B, Russell JW. Insulin-like growth factors regulate neuronal differentiation and survival. *Neurobiol Dis*. 1997;4:201–214.
78 Yoshikawa S, Taniguchi K, Sawamura H, et al. Metabolic associated fatty liver disease as a risk factor for the development of central nervous system disorders. *Livers*. 2023;3:21–32.
79 Pasmans K, Adriaens ME, Olinga P, et al. Hepatic steatosis contributes to the development of muscle atrophy via inter-organ crosstalk. *Front Endocrinol*. 2021;12:733625.
80 Srikanthan P, Karlamangla AS. Relative muscle mass is inversely associated with insulin resistance and prediabetes. Findings from the third National Health and Nutrition Examination Survey. *J Clin Endocrinol Metab*. 2011;96:2898–2903.
81 De Bandt JP, Jegatheesan P, Tennoune-El-Hafaia N. Muscle loss in chronic liver diseases: the example of nonalcoholic liver disease. *Nutrients*. 2018;10:1195.
82 Hora S, Wuestefeld T. Liver injury and regeneration: current understanding, new approaches, and future perspectives. *Cells*. 2023;12:2129.
83 Reilly A, Yaworski R, Beauvais A, Schneider BL, Kothary R. Long term peripheral AAV9-SMN gene therapy promotes survival in a mouse model of spinal muscular atrophy. *Hum Mol Genet*. 2024;33:510–519.
84 Bowerman M, Becker CG, Yáñez-Muñoz RJ, et al. Therapeutic strategies for spinal muscular atrophy: SMN and beyond. *Dis Model Mech*. 2017;10:943–954.
85 Day JW, Howell K, Place A, et al. Advances and limitations for the treatment of spinal muscular atrophy. *BMC Pediatr*. 2022;22:632.